Journal of
Mechanics of
Materials and Structures

IMPROVED SMEARED AND ZIGZAG THIRD-ORDER THEORIES FOR PIEZOELECTRIC ANGLE-PLY LAMINATED CYLINDRICAL SHELLS UNDER ELECTROTHERMOMECHANICAL LOADS

Jayanta Kumar Nath and Santosh Kapuria

Volume 4, Nº 6 June 2009

mathematical sciences publishers

JOURNAL OF MECHANICS OF MATERIALS AND STRUCTURES
Vol. 4, No. 6, 2009

IMPROVED SMEARED AND ZIGZAG THIRD-ORDER THEORIES FOR PIEZOELECTRIC ANGLE-PLY LAMINATED CYLINDRICAL SHELLS UNDER ELECTROTHERMOMECHANICAL LOADS

JAYANTA KUMAR NATH AND SANTOSH KAPURIA

An improved efficient zigzag theory (IZIGT) and an improved third-order theory (ITOT) are presented for hybrid piezoelectric angle-ply composite circular cylindrical shells under electrothermomechanical loading. In both theories, the potential and thermal fields are approximated as piecewise linear across a number of sublayers so that the nonlinear potential field and actual temperature profile across the laminate thickness can be captured to any desired degree of accuracy. The transverse displacement is approximated to explicitly account for the transverse normal strain resulting from thermal and electric fields without introducing additional unknowns. The shear traction free conditions on the top and bottom surfaces in both theories and the continuity of transverse shear stresses at layer interfaces in the IZIGT are satisfied exactly considering coupled constitutive equations. The theories are assessed in comparison with the available exact 3D piezothermoelasticity solution for simply supported angle-ply hybrid cylindrical panels under electrothermomechanical loads. The comparisons for a hybrid test panel, a composite panel, and a sandwich panel establish that the IZIGT is very accurate and the ITOT is an improvement over the conventional third-order theory for thermal loads, which assumes uniform deflection across the laminate thickness.

1. Introduction

Research efforts continue to be directed towards the analysis, design, development, and testing of smart piezoelectric composite shell-type structures because of the increasing potential of their use in aerospace, marine, and automobile vehicles. Due to the presence of high layerwise inhomogeneity in mechanical, thermal and electric properties in these so called hybrid laminates, development of an accurate but computationally efficient two-dimensional (2D) shell theory for their analysis is a requirement that poses considerable challenges. Exact three-dimensional (3D) piezothermoelasticity solutions for simply supported finite-length cross-ply hybrid cylindrical shells [Xu and Noor 1996; Kapuria et al. 1997] and for infinite-length angle-ply hybrid cylindrical shells [Dumir et al. 1997] have been presented, against which the accuracy of the 2D theories can be assessed. In 3D solutions, no simplified hypothesis is made on the variations of field variables along the thickness coordinate, whereas in 2D laminate theories, variables are approximated in the thickness direction assuming a priori a given expansion. It is now well understood that:

- The neglect of direct piezoelectric and pyroelectric coupling effects leads to substantial error in predicting structural response [Lee and Saravanos 2000].

Keywords: cylindrical shell, angle-ply, piezoelectric composite, zigzag theory, thermal load.

- The transverse normal strain (out-of-plane deformation) can not be neglected in presence of thermal and electric fields [Kapuria and Achary 2006].
- The slope discontinuity in the inplane displacements at the layer interfaces, as observed from exact 3D solutions [Kapuria et al. 1997] should be included in the 2D theory for obtaining an accurate response.
- A 2D theory which works well for a shell loaded by an assumed linear or quadratic temperature profile may yield inaccurate results for an actual temperature profile based on the heat conduction equation [Carrera 2002].

These effects should be included in an accurate 2D theory, without enhancing the cost of analysis.

A comprehensive review of the 2D theories for piezoelectric hybrid plates and shells has been presented by Saravanos and Heyliger [1999]. Classical laminate theory (CLT) has been employed for electromechanical static and dynamic response of piezoelectric laminated generic [Jia and Rogers 1990] and circular cylindrical [Sung et al. 1996; Zhang et al. 2008] shells, wherein the two-way electromechanical coupling is not considered (the charge balance equation is not solved). Kapuria et al. [1998b] presented an assessment of uncoupled CLT and first-order shear deformation theory (FSDT) based on Flugge's approximations for electromechanical response of hybrid circular cylindrical shells in direct comparison with the exact 3D piezoelasticity solution. Berg et al. [2004] employed classical shell theory based on Flugge's approximations for the dynamic response of single-layer piezoelectric shells, considering electromechanical coupling. A coupled mixed field approach [Saravanos 1997; Saravanos and Christoforou 2002] with FSDT assumptions for the displacement field and layerwise linear approximation for the electric potential has been employed for doubly curved and cylindrical hybrid shells. Pinto Correia et al. [2002] developed a finite element for active control of axisymmetric hybrid shells based on the coupled third-order theory (TOT) with a sublayerwise linear approximation for electric potential. In this theory, the shear traction conditions at the top (outer) and bottom (inner) surfaces of the shell are not satisfied in presence of nonuniform electric potential on these surfaces. These equivalent single layer (ESL) theories, wherein the displacements are assumed to follow a global variation across the laminate thickness, violate the slope discontinuity in the inplane displacements and continuity of transverse shear stresses at the layer interfaces. The slope discontinuity is incorporated in the displacement field approximations of the layerwise theories (LWT), which yield accurate results [D'Ottavio et al. 2006; Carrera and Brischetto 2007]. However, these are computationally expensive since the number of unknown variables increases with the number of layers, which restricts their applicability in dynamics and control problems. As an efficient alternative to the LWT, zigzag theories (ZIGT) have been proposed, wherein the assumptions of displacements are the same as in the LWT with additional quadratic and cubic or trigonometric global variation across thickness for the inplane displacements. But the number of variables is reduced to that of the corresponding ESL theory by enforcing transverse shear continuity conditions at layer interfaces, and shear traction free conditions at the top and bottom surfaces. Ossadzow-David and Touratier [2004] presented a semicoupled ZIGT for doubly curved hybrid shells under electromechanical loading wherein the continuity and boundary conditions on transverse shear stresses and transverse electric displacement at the layer interfaces and the bounding surfaces (top and bottom) are satisfied using uncoupled constitutive equations. D'Ottavio et al. [2006] and Carrera and Brischetto [2007] also employed ESL models

with additional Murakami zigzag functions for inplane displacements, which do not satisfy the conditions on transverse shear stresses.

Limited literature is available wherein the above theories have been extended to incorporate thermal loading and the implications of the thermal effects on the hybrid shells have been assessed. The uncoupled CLT [Tzou and Bao 1995], coupled mixed field FSDT with layerwise linear potential [Raja et al. 2004], and coupled ZIGT [Kim et al. 2002; Oh and Cho 2007] have been presented for doubly curved shells under assumed temperature profile of linear and cubic variations across the thickness. A finite element model based on the coupled FSDT with layerwise linear temperature profile was presented for doubly curved hybrid shells by Lee and Saravanos [2000]. Kapuria et al. [1998a] extended the uncoupled CLT and FSDT based on Flugge's approximations for hybrid cylindrical shells to the thermal load case with layerwise temperature profile and assessed the theories in direct comparison with the 3D exact piezothermoelasticity solution. Such comparisons are not available for the other advanced 2D theories for hybrid shells under thermoelectric loading.

In this work, two new improved 2D theories are developed, namely, improved zigzag theory (IZIGT) and improved third-order theory (ITOT) for hybrid piezoelectric angle-ply composite cylindrical shells under electrothermomechanical loading. It is an extension an earlier work [Kapuria and Achary 2006; Kumari et al. 2008] for hybrid plates to the case of hybrid cylindrical shells. The temperature field is approximated to be piecewise linear across a number of sublayers across the laminate so as to capture the actual thermal profile based on the heat conduction equation, to any desired accuracy. The electric potential is similarly approximated across the piezoelectric layers, and the deflection is approximated to account for the normal strain along the thickness direction due to thermal and electric fields, without introducing any additional unknown variables. The conditions on transverse shear stresses at the top and bottom and at the layer interfaces (for IZIGT only) are satisfied exactly considering the coupled constitutive equations, and the number of displacement unknowns in both theories is reduced to five. The theories are assessed in direct comparison with the exact piezothermoelasticity solution [Dumir et al. 1997] for simply supported angle-ply infinite-length hybrid cylindrical panels of heterogeneous composite and sandwich laminate configurations under mechanical, electric potential, and thermal loads. The effect of inclusion of transverse normal strain in the approximation of deflection is investigated.

2. Displacement, potential and thermal field approximations

Consider a hybrid circular cylindrical shell panel of thickness h and circumferential span angle α as shown in Figure 1, with circumferential axis θ, longitudinal axis x, and thickness (radial) axis z. It is made of L number of perfectly bonded orthotropic layers with their stiffer principal material axis direction at an angle ψ to the θ-axis. Some of the layers can be of radially polarized piezoelectric materials of orthorhombic class mm2 symmetry [Auld 1973]. The shell is subjected to a thermal load and a transverse mechanical load on the inner (bottom) and the outer (top) surfaces, with actuation potentials applied to some piezoelectric layers. The midsurface of the panel is chosen as the reference surface $z = 0$. The z-coordinate of the bottom surface of the k-th layer from the bottom is denoted as z_{k-1}. Thus, the z-coordinates of the bottom and the top surfaces are z_0 and z_L, respectively, with $z_0 = -h/2$ and $z_L = h/2$. The layer in which the reference surface lies or is at the bottom is denoted as the k_0-th layer and its radius is R.

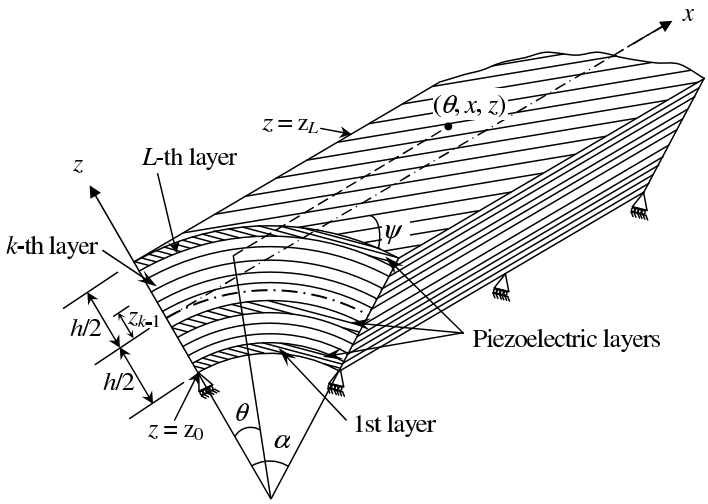

Figure 1. Geometry of a hybrid angle-ply cylindrical shell.

The 3D piezothermoelasticity solutions [Kapuria et al. 1997] have revealed that the contribution of the transverse normal stress σ_z to the strain energy is much smaller than the contributions of the other stress components. Hence the assumption of $\sigma_z \simeq 0$ made in some 2D shell theories is retained in the present formulation. Using this assumption, the linear constitutive equations for the stresses σ_θ, σ_x, $\tau_{\theta x}$, τ_{xz}, and $\tau_{\theta z}$ and the electric displacements D_θ, D_x, and D_z are given by

$$\sigma = \bar{Q}\varepsilon - \bar{e}_3^{\mathrm{T}} E_z - \bar{\beta} T, \qquad \tau = \hat{Q}\gamma - \hat{e}E \qquad D = \hat{e}^{\mathrm{T}}\gamma + \hat{\eta}E, \qquad D_z = \bar{e}_3\varepsilon + \bar{\eta}_{33}E_z + \bar{p}_3 T, \tag{1}$$

where

$$\sigma = \begin{bmatrix} \sigma_\theta \\ \sigma_x \\ \tau_{\theta x} \end{bmatrix}, \quad \tau = \begin{bmatrix} \tau_{\theta z} \\ \tau_{xz} \end{bmatrix}, \quad D = \begin{bmatrix} D_\theta \\ D_x \end{bmatrix}, \quad \varepsilon = \begin{bmatrix} \varepsilon_\theta \\ \varepsilon_x \\ \gamma_{\theta x} \end{bmatrix},$$
$$\bar{Q} = \begin{bmatrix} \bar{Q}_{11} & \bar{Q}_{12} & \bar{Q}_{16} \\ \bar{Q}_{12} & \bar{Q}_{22} & \bar{Q}_{26} \\ \bar{Q}_{16} & \bar{Q}_{26} & \bar{Q}_{66} \end{bmatrix}, \quad \bar{\beta} = \begin{bmatrix} \bar{\beta}_1 \\ \bar{\beta}_2 \\ \bar{\beta}_6 \end{bmatrix}, \quad \gamma = \begin{bmatrix} \gamma_{\theta z} \\ \gamma_{xz} \end{bmatrix}, \quad \hat{Q} = \begin{bmatrix} \bar{Q}_{55} & \bar{Q}_{45} \\ \bar{Q}_{45} & \bar{Q}_{44} \end{bmatrix}, \tag{2}$$
$$E = \begin{bmatrix} E_\theta \\ E_x \end{bmatrix}, \quad \hat{e} = \begin{bmatrix} \bar{e}_{15} & \bar{e}_{25} \\ \bar{e}_{14} & \bar{e}_{24} \end{bmatrix}, \quad \hat{\eta} = \begin{bmatrix} \bar{\eta}_{11} & \bar{\eta}_{12} \\ \bar{\eta}_{12} & \bar{\eta}_{22} \end{bmatrix}, \quad \bar{e}_3 = \begin{bmatrix} \bar{e}_{31} & \bar{e}_{32} & \bar{e}_{36} \end{bmatrix}.$$

Here ε and γ are the inplane and transverse strain components, and E_θ, E_x, and E_z are the electric field components. $\bar{Q}_{ij}$, $\bar{e}_{ij}$, $\bar{\eta}_{ij}$, and $\bar{\beta}_i$ are the reduced elastic stiffnesses, piezoelectric stress constants, electric permittivities, and stress-temperature coefficients, respectively. Let u_θ, u_x, and w be the inplane and transverse displacements and ϕ be the electric potential. Denoting differentiation by a subscript comma, the strain-displacement and electric field-electric potential relations for small strain condition

are given by

$$\begin{aligned} \varepsilon_\theta &= \frac{u_{\theta,\theta}+w}{R+z}, & \gamma_{xz} &= u_{x,z}+w_{,x}, & E_\theta &= -\frac{\phi_{,\theta}}{R+z}, \\ \varepsilon_x &= u_{x,x}, & \gamma_{\theta z} &= u_{\theta,z}+\frac{w_{,\theta}-u_\theta}{R+z}, & E_x &= -\phi_{,x}, \\ \varepsilon_z &= w_{,z}, & \gamma_{\theta x} &= u_{\theta,x}+\frac{u_{x,\theta}}{R+z}, & E_z &= -\phi_{,z}. \end{aligned} \tag{3}$$

The temperature field $T(\theta, x, z)$ for the hybrid laminated shell can be solved analytically for some geometries or numerically by, say, the finite element method. The temperature field T is approximated piecewise linearly between n_T points at z_T^l $(l = 1, 2, \ldots, n_T)$ across the thickness. The potential field is similarly approximated between n_ϕ points at z_ϕ^j $(j = 1, 2, \ldots, n_\phi)$ across the thickness:

$$T(\theta, x, z) = \Psi_T^l(z)T^l(\theta, x), \qquad \phi(\theta, x, z) = \Psi_\phi^j(z)\phi^j(\theta, x), \tag{4}$$

where $T^l(\theta, x) = T(\theta, x, z_T^l)$ and $\phi^j(\theta, x) = \phi(\theta, x, z_\phi^j)$. Functions $\Psi_T^l(z)$ and $\Psi_\phi^j(z)$ are linear Lagrange interpolation functions for T and ϕ respectively. The summation convention is used for repeated indices l and j, and for l' and j', used later. For discretisation of T and ϕ, each layer is divided into a number of sublayers as required by the desired accuracy.

3D exact solutions [Xu and Noor 1996; Kapuria et al. 1997] have revealed that for moderately thick hybrid shells under thermoelectric load, the transverse displacement w has significant variation across the thickness, which is caused by the thickness deformation primarily due to the electric and thermal fields. Hence, in the present IZIGT, w is approximated by neglecting the contributions of stresses in the constitutive equation for ε_z, but retaining the contributions of thermal and electric fields and then integrating the remaining expression for ε_z:

$$\varepsilon_z = w_{,z} \simeq -\bar{d}_{33}\phi_{,z} + \bar{\alpha}_3 T \quad \Longrightarrow \quad w(\theta, x, z) = w_0(\theta, x) - \bar{\Psi}_\phi^j(z)\phi^j(\theta, x) + \bar{\Psi}_T^l(z)T^l(\theta, x), \tag{5}$$

with

$$\bar{\Psi}_\phi^j(z) = \int_0^z d_{33}\Psi_{\phi,z}^j(z)\,dz, \qquad \bar{\Psi}_T^l(z) = \int_0^z \alpha_3\Psi_T^l(z)\,dz. \tag{6}$$

$\bar{\Psi}_\phi^j(z)$ is a piecewise linear function and $\bar{\Psi}_T^l(z)$ is a piecewise quadratic function.

The inplane displacements u_θ and u_x are approximated as a combination of a global third-order variation in z across the thickness and a layerwise piecewise linear variation:

$$u(\theta, x, z) = \begin{bmatrix} 1+\dfrac{z}{R} & 0 \\ 0 & 1 \end{bmatrix} u_k(\theta, x) - z w_{0_d} + z\psi_k(\theta, x) + z^2\xi(\theta, x) + z^3\eta(\theta, x) \tag{7}$$

where

$$u = \begin{bmatrix} u_\theta \\ u_x \end{bmatrix}, \quad u_k = \begin{bmatrix} u_{k_\theta} \\ u_{k_x} \end{bmatrix}, \quad w_{0_d} = \begin{bmatrix} w_{0,\theta}/R \\ w_{0,x} \end{bmatrix}, \quad \psi_k = \begin{bmatrix} \psi_{k_\theta} \\ \psi_{k_x} \end{bmatrix}, \quad \xi = \begin{bmatrix} \xi_\theta \\ \xi_x \end{bmatrix}, \quad \eta = \begin{bmatrix} \eta_\theta \\ \eta_x \end{bmatrix}, \tag{8}$$

and u_k and ψ_k are the translation and shear rotation variables of the k-th layer. Substituting u_θ and u_x from (7), w from (5) and ϕ from $(4)_2$ into (3) and thereafter using (1), the transverse shear stresses τ are

obtained as

$$\tau = Q_1^k(z)\psi_k + Q_2^k(z)\xi + Q_3^k(z)\eta + Q_{4j}^k(z)\phi_d^j + Q_{5l}^k(z)T_d^l, \tag{9}$$

with

$$Q_1^k(z) = \hat{Q}^k \begin{bmatrix} \frac{R}{R+z} & 0 \\ 0 & 1 \end{bmatrix}, \quad Q_{5l}^k(z) = \hat{Q}^k \begin{bmatrix} \frac{R}{R+z} & 0 \\ 0 & 1 \end{bmatrix} \bar{\Psi}_T^l(z), \quad Q_2^k(z) = \hat{Q}^k \begin{bmatrix} \frac{z^2+2zR}{R+z} & 0 \\ 0 & 2z \end{bmatrix},$$

$$\phi_d^j = \begin{bmatrix} \frac{\phi_{,\theta}^j}{R} \\ \phi_{,x}^j \end{bmatrix}, \quad Q_3^k(z) = \hat{Q}^k \begin{bmatrix} \frac{2z^3+3z^2R}{R+z} & 0 \\ 0 & 3z^2 \end{bmatrix}, \quad T_d^l = \begin{bmatrix} \frac{T_{,\theta}^l}{R} \\ T_{,x}^l \end{bmatrix}, \tag{10}$$

$$Q_{4j}^k(z) = \hat{e}^k \begin{bmatrix} \frac{R}{R+z} & 0 \\ 0 & 1 \end{bmatrix} \Psi_\phi^j(z) - \hat{Q}^k \begin{bmatrix} \frac{R}{R+z} & 0 \\ 0 & 1 \end{bmatrix} \bar{\Psi}_\phi^j(z).$$

The conditions of zero transverse shear stresses τ at the inner and outer surfaces, and the continuity of τ and u at the layer interfaces yield

$$\tau(z_0) = 0 \implies Q_1^1(z_0)\psi_1 + Q_2^1(z_0)\xi + Q_3^1(z_0)\eta = -Q_{4j}^1(z_0)\phi_d^j - Q_{5l}^1(z_0)T_d^l, \tag{11}$$

$$\tau(z_k^-) = \tau(z_k^+) \implies Q_1^{k+1}(z_k)\psi_{k+1} - Q_1^k(z_k)\psi_k + \hat{Q}_2^k\xi + \hat{Q}_3^k\eta = -\hat{Q}_{4j}^k\phi_d^j - \hat{Q}_{5l}^k T_d^l, \tag{12}$$

$$u(z_k^-) = u(z_k^+) \implies \begin{bmatrix} 1+\frac{z_k}{R} & 0 \\ 0 & 1 \end{bmatrix} (u_{k+1} - u_k) + z_k\psi_{k+1} - z_k\psi_k = 0, \tag{13}$$

$$\tau(z_L) = 0 \implies Q_1^L(z_L)\psi_L + Q_2^L(z_L)\xi + Q_3^L(z_L)\eta = -Q_{4j}^L(z_L)\phi_d^j - Q_{5l}^L(z_L)T_d^l, \tag{14}$$

where $k = 1, \ldots, L-1$,

$$\hat{Q}_i^k = Q_i^{k+1}(z_k) - Q_i^k(z_k), \quad i = 1, 2, 3, 4, \tag{15}$$

and

$$\hat{Q}_{4j}^k = Q_{4j}^{k+1}(z_k) - Q_{4j}^k(z_k), \qquad \hat{Q}_{5l}^k = Q_{5l}^{k+1}(z_k) - Q_{5l}^k(z_k). \tag{16}$$

Equations (11)–(14) along with $u_{k_0} = u_0$ and $\psi_{k_0} = \psi_0$ are arranged in matrix form for the $2L+2$ unknowns u_k, ψ_k, ξ, and η:

$$A\bar{x} = B^u u_0 + B^\psi \psi_0 + B_j^\phi \phi_d^j + B_l^T T_d^l, \tag{17}$$

where A is a $(4L+4) \times (4L+4)$ matrix, B^u, B^ψ, B_j^ϕ, and B_l^T are matrices of size $(4L+4) \times 2$, and

$$\bar{x} = \begin{bmatrix} u_1^{\mathrm{T}} & \psi_1^{\mathrm{T}} & u_2^{\mathrm{T}} & \psi_2^{\mathrm{T}} & \ldots & u_L^{\mathrm{T}} & \psi_L^{\mathrm{T}} & \xi^{\mathrm{T}} & \eta^{\mathrm{T}} \end{bmatrix}^{\mathrm{T}}. \tag{18}$$

Partitioning the matrices A, B^u, B^ψ, B_j^ϕ, and B_l^T into 2×2 submatrices $A(i,j)$, $B^u(i)$, $B^\psi(i)$, $B_j^\phi(i)$, and $B_l^T(i)$, the nonzero submatrices are given by

$$
\begin{aligned}
A(1,2) &= Q_1^1(z_0), & A(2L,2L) &= Q_1^L(z_L), & B^u(2L+1) &= I_2,\\
A(1,2L+1) &= Q_2^1(z_0), & A(2L,2L+1) &= Q_2^L(z_L), & B^\psi(2L+2) &= I_2,\\
A(1,2L+2) &= Q_3^1(z_0), & A(2L,2L+2) &= Q_3^L(z_L), & B_j^\phi(1) &= -Q_{4j}^1(z_0),\\
A(2i,2i) &= -Q_1^i(z_i), & A(2L+1,2k_0-1) &= I_2, & B_j^\phi(2i) &= -\hat{Q}_{4j}^i(z_i),\\
A(2i,2i+2) &= Q_1^{i+1}(z_i), & A(2L+2,2k_0) &= I_2, & B_j^\phi(2L) &= -Q_{4j}^L(z_L),\\
A(2i,2L+2) &= \hat{Q}_3^i(z_i), & A(2i+1,2i) &= -z_i I_2, & B_l^T(1) &= -Q_{5l}^1(z_0),\\
A(2i,2L+1) &= \hat{Q}_2^i(z_i), & A(2i+1,2i+2) &= z_i I_2, & B_l^T(2i) &= -\hat{Q}_{5l}^i(z_i),\\
A(2i+1,2i-1) &= -\begin{bmatrix} 1+\frac{z_i}{R} & 0\\ 0 & 1\end{bmatrix}, & A(2i+1,2i+1) &= \begin{bmatrix} 1+\frac{z_i}{R} & 0\\ 0 & 1\end{bmatrix}, & B_l^T(2L) &= -Q_{5l}^L(z_L),
\end{aligned}
$$

for $i=1,\ldots,L-1$. Here I_2 is the 2×2 identity matrix. The solution of (17) can be expressed as

$$\bar{x} = C^u u_0 + C^\psi \psi_0 + C_j^\phi \phi_d^j + C_l^T T_d^l, \tag{19}$$

where

$$C^u = A^{-1}B^u, \qquad C^\psi = A^{-1}B^\psi, \qquad C_j^\phi = A^{-1}B_j^\phi, \qquad C_l^T = A^{-1}B_l^T. \tag{20}$$

C^u, C^ψ, C_j^ϕ, and C_l^T are partitioned into $2L+1$ submatrices $C^u(i)$, $C^\psi(i)$, $C_j^\phi(i)$, and $C_l^T(i)$ of size 2×2 each. Since ξ, η, and ψ_i in (11), (12), and (14) can be solved in terms of ψ_0, ϕ_d^j, and T_d^l only, it follows that $C^u(2i)=0$ for $i=1,\ldots,L$, and $C^u(2L+1)=C^u(2L+2)=0$. Moreover, (13) implies that $u_i = u_0 + f(\psi_1,\psi_2,\ldots,\psi_L)$, where f is a function of the ψ_i. Thus $C^u(2i-1)=I_2$. Considering these submatrices of C, (19) can be explicitly written as

$$
\begin{aligned}
u_k &= I_2 u_0 + C^\psi(2k-1)\psi_0 + C_j^\phi(2k-1)\phi_d^j + C_l^T(2k-1)T_d^l,\\
\psi_k &= C^\psi(2k)\psi_0 + C_j^\phi(2k)\phi_d^j + C_l^T(2k)T_d^l,\\
\xi &= C^\psi(2L+1)\psi_0 + C_j^\phi(2L+1)\phi_d^j + C_l^T(2L+1)T_d^l,\\
\eta &= C^\psi(2L+2)\psi_0 + C_j^\phi(2L+2)\phi_d^j + C_l^T(2L+2)T_d^l.
\end{aligned}
\tag{21}
$$

These expressions are now substituted in (7) to obtain the final expressions of u:

$$u(\theta,x,z) = \begin{bmatrix} 1+\frac{z}{R} & 0\\ 0 & 1\end{bmatrix} u_0(\theta,x) - z w_{0_d}(\theta,x) + R^k(z)\psi_0(\theta,x) + \hat{R}^{kj}(z)\phi_d^j(\theta,x) + \bar{R}^{kl}(z)T_d^l(\theta,x), \tag{22}$$

where

$$
\begin{aligned}
R^k(z) &= R_1^k + zR_2^k + z^2R_3 + z^3R_4,\\
\hat{R}^{kj}(z) &= \hat{R}_1^{kj} + z\hat{R}_2^{kj} + z^2\hat{R}_3^j + z^3\hat{R}_4^j,\\
\bar{R}^{kl}(z) &= \bar{R}_1^{kl} + z\bar{R}_2^{kl} + z^2\bar{R}_3^l + z^3\bar{R}_4^l,
\end{aligned}
\tag{23}
$$

with

$$R_1^k = C^\psi(2k-1),\quad R_2^k = \begin{bmatrix} \frac{1}{R} & 0 \\ 0 & 0 \end{bmatrix} C^\psi(2k-1) + C^\psi(2k),\quad R_3 = C^\psi(2L+1),\quad R_4 = C^\psi(2L+2),$$
$$\hat{R}_1^{kj} = C_j^\phi(2k-1),\quad \hat{R}_2^{kj} = \begin{bmatrix} \frac{1}{R} & 0 \\ 0 & 0 \end{bmatrix} C_j^\phi(2k-1) + C_j^\phi(2k),\quad \hat{R}_3^j = C_j^\phi(2L+1),\quad \hat{R}_4^j = C_j^\phi(2L+2), \tag{24}$$
$$\bar{R}_1^{kl} = C_l^T(2k-1),\quad \bar{R}_2^{kl} = \begin{bmatrix} \frac{1}{R} & 0 \\ 0 & 0 \end{bmatrix} C_l^T(2k-1) + C_l^T(2k),\quad \bar{R}_3^l = C_l^T(2L+1),\quad \bar{R}_4^l = C_l^T(2L+2).$$

For the improved and consistent third-order ESL theory (ITOT), w is approximated by (5) and u is approximated as

$$u(\theta, x, z) = \begin{bmatrix} 1+\frac{z}{R} & 0 \\ 0 & 1 \end{bmatrix} u_0(\theta, x) - z w_{0_d} + z\psi_0(\theta, x) + z^2\xi(\theta, x) + z^3\eta(\theta, x), \tag{25}$$

for which the expression for τ is obtained as

$$\tau = Q_1^k(z)\psi_0 + Q_2^k(z)\xi + Q_3^k(z)\eta + Q_{4j}^k(z)\phi_d^j + Q_{5l}^k(z)T_d^l. \tag{26}$$

Applying the shear traction-free condition $\tau = 0$ at $z = z_0, z_L$ yields

$$\bar{a}_1\psi_0 + \bar{a}_2\xi + \bar{a}_3\eta + \bar{a}_{4j}\phi_d^j + \bar{a}_{5l}T_d^l = 0, \qquad \bar{b}_1\psi_0 + \bar{b}_2\xi + \bar{b}_3\eta + \bar{b}_{4j}\phi_d^j + \bar{b}_{5l}T_d^l = 0, \tag{27}$$

where

$$\begin{aligned} &\bar{a}_1 = Q_1^1(z_0), \quad \bar{a}_2 = Q_2^1(z_0), \quad \bar{a}_3 = Q_3^1(z_0), \quad \bar{a}_{4j} = Q_{4j}^1(z_0), \quad \bar{a}_{5l} = Q_{5l}^1(z_0), \\ &\bar{b}_1 = Q_1^L(z_L), \quad \bar{b}_2 = Q_2^L(z_L), \quad \bar{b}_3 = Q_3^L(z_L), \quad \bar{b}_{4j} = Q_{4j}^L(z_L), \quad \bar{b}_{5l} = Q_{5l}^L(z_L). \end{aligned} \tag{28}$$

Equation (27) is solved for ξ and η to obtain

$$\xi = R_3\psi_0 + \hat{R}_3^j\phi_d^j + \bar{R}_3^l T_d^l, \qquad \eta = R_4\psi_0 + \hat{R}_4^j\phi_d^j + \bar{R}_4^l T_d^l, \tag{29}$$

where

$$\begin{aligned} &R_3 = \bar{\Delta}^{-1}(\bar{b}_3^{-1}\bar{b}_1 - \bar{a}_3^{-1}\bar{a}_1), \qquad R_4 = -\bar{a}_3^{-1}(\bar{a}_2 R_3 + \bar{a}_1), \\ &\hat{R}_3^j = \bar{\Delta}^{-1}(\bar{b}_3^{-1}\bar{b}_{4j} - \bar{a}_3^{-1}\bar{a}_{4j}), \qquad \hat{R}_4^j = -\bar{a}_3^{-1}(\bar{a}_2\hat{R}_3^j + \bar{a}_{4j}), \\ &\bar{R}_3^l = \bar{\Delta}^{-1}(\bar{b}_3^{-1}\bar{b}_{5l} - \bar{a}_3^{-1}\bar{a}_{5l}), \qquad \bar{R}_4^l = -\bar{a}_3^{-1}(\bar{a}_2\bar{R}_3^l + \bar{a}_{5l}), \qquad \bar{\Delta} = \bar{a}_3^{-1}\bar{a}_2 - \bar{b}_3^{-1}\bar{b}_2. \end{aligned} \tag{30}$$

Substitution of ξ and η from (29) into (25) yields the expression of u for the ITOT to be of the same form as of (22) for the IZIGT with the functions $R^k(z)$, $\hat{R}^{kj}(z)$, and $\bar{R}^{kl}(z)$ for the former given by

$$R^k(z) = zI_2 + z^2R_3 + z^3R_4, \qquad \hat{R}^{kj}(z) = z^2\hat{R}_3^j + z^3\hat{R}_4^j, \qquad \bar{R}^{kl}(z) = z^2\bar{R}_3^l + z^3\bar{R}_4^l. \tag{31}$$

3. Strain-displacement relations

The displacements u and w given by (22), (5) and the small virtual displacements $\delta u, \delta w$ can be written

$$u = f_1(z)\bar{u}_1 + \bar{R}^{kl}(z)T_d^l, \qquad w = f_2(z)\bar{u}_2 + \bar{\Psi}_T^l(z)T^l, \tag{32}$$

$$\delta u = f_1(z)\delta\bar{u}_1 = \delta\bar{u}_1^{\mathrm{T}} f_1^{\mathrm{T}}(z), \qquad \delta w = f_2(z)\delta\bar{u}_2 = \delta\bar{u}_2^{\mathrm{T}} f_2^{\mathrm{T}}(z), \tag{33}$$

with

$$\bar{u}_1 = \left[u_0^{\mathrm{T}} \ -w_{0_d}^{\mathrm{T}} \ \psi_0^{\mathrm{T}} \ \phi_d^{j\,\mathrm{T}}\right]^{\mathrm{T}}, \qquad \bar{u}_2 = \left[w_0 \ -\phi^j\right]^{\mathrm{T}}, \qquad I_z = \begin{bmatrix} 1+\frac{z}{R} & 0 \\ 0 & 1 \end{bmatrix},$$
$$f_1(z) = \left[I_z \ I_2 z \ R^k(z) \ \hat{R}^{kj}(z)\right], \qquad f_2(z) = \left[1 \ \bar{\Psi}_\phi^j(z)\right], \tag{34}$$

where the index j indicates a sequence of elements with j ranging from 1 to n_ϕ. Substituting u and w from (22) and (5) into (3) yields

$$\varepsilon = f_3(z)\bar{\varepsilon}_1 + \bar{f}_2(z)\bar{u}_2 + \bar{\Phi}^{kl}(z)T_{dd}^l + \tilde{I}_1(z)\bar{\Psi}_T^l(z)T^l, \qquad \gamma = f_4(z)\bar{\varepsilon}_2 + \bar{\Phi}_0^{kl}(z)T_d^l, \tag{35}$$

and hence

$$\delta\varepsilon = f_3(z)\delta\bar{\varepsilon}_1 + \bar{f}_2(z)\delta\bar{u}_2, \quad \delta\gamma = f_4(z)\delta\bar{\varepsilon}_2, \tag{36}$$

with

$$f_3(z) = \left[\Phi^0(z) \ \Phi(z) \ \Phi^k(z) \ \Phi^{kj}(z)\right], \quad f_4(z) = \left[\Phi_0^k(z) \ \Phi_0^{kj}(z)\right], \quad \bar{f}_2(z) = \frac{1}{R+z}\bar{I}_1\left[1 \ \bar{\Psi}_\phi^j(z)\right], \tag{37}$$

$$\Phi^0(z) = \begin{bmatrix} 1 & 0 & 0 & 0 \\ 0 & 0 & 0 & 1 \\ 0 & 1+\frac{z}{R} & \frac{1}{1+z/R} & 0 \end{bmatrix}, \qquad \Phi(z) = \begin{bmatrix} \frac{z}{1+z/R} & 0 & 0 & 0 \\ 0 & 0 & 0 & z \\ 0 & z & \frac{z}{1+z/R} & 0 \end{bmatrix},$$

$$\Phi^k(z) = \begin{bmatrix} \frac{R_{11}^k}{1+z/R} & 0 & \frac{R_{12}^k}{1+z/R} & 0 \\ 0 & R_{21}^k & 0 & R_{22}^k \\ \frac{R_{21}^k}{1+z/R} & R_{11}^k & \frac{R_{22}^k}{1+z/R} & R_{12}^k \end{bmatrix}, \qquad \Phi^{kj}(z) = \begin{bmatrix} \frac{R_{11}^{kj}}{1+z/R} & 0 & \frac{R_{12}^{kj}}{1+z/R} & 0 \\ 0 & R_{21}^{kj} & 0 & R_{22}^{kj} \\ \frac{R_{21}^{kj}}{1+z/R} & R_{11}^{kj} & \frac{R_{22}^{kj}}{1+z/R} & R_{12}^{kj} \end{bmatrix}, \tag{38}$$

$$\Phi_0^k(z) = \begin{bmatrix} R_{11,z}^k - \frac{R_{11}^k}{R+z} & R_{12,z}^k - \frac{R_{12}^k}{R+z} \\ R_{21,z}^k & R_{22,z}^k \end{bmatrix}, \qquad \bar{\Phi}^{kl}(z) = \begin{bmatrix} \frac{\bar{R}_{11}^{kl}}{1+z/R} & 0 & \frac{\bar{R}_{12}^{kl}}{1+z/R} & 0 \\ 0 & \bar{R}_{21}^{kl} & 0 & \bar{R}_{22}^{kl} \\ \frac{\bar{R}_{21}^{kl}}{1+z/R} & \bar{R}_{11}^{kl} & \frac{\bar{R}_{22}^{kl}}{1+z/R} & \bar{R}_{12}^{kl} \end{bmatrix},$$

$$\Phi_0^{kj}(z) = \begin{bmatrix} R_{11,z}^{kj} - \frac{R_{11}^{kj} + R\bar{\Psi}_\phi^j}{R+z} & R_{12,z}^{kj} - \frac{R_{12}^{kj}}{R+z} \\ R_{21,z}^{kj} & R_{22,z}^{kj} - \bar{\Psi}_\phi^j \end{bmatrix}, \qquad \bar{\Phi}_0^{kl}(z) = \begin{bmatrix} \bar{R}_{11,z}^{kl} - \frac{\bar{R}_{11}^{kl} - R\bar{\Psi}_T^l}{R+z} & \bar{R}_{12,z}^{kl} - \frac{\bar{R}_{12}^{kl}}{R+z} \\ \bar{R}_{21,z}^{kl} & \bar{R}_{22,z}^{kl} + \bar{\Psi}_T^l \end{bmatrix},$$

$$\bar{\varepsilon}_1 = \begin{bmatrix} u_{0_d} \\ -w_{0_{dd}} \\ \psi_{0_d} \\ \phi^j_{dd} \end{bmatrix}, \quad \bar{\varepsilon}_2 = \begin{bmatrix} \psi_0 \\ \phi^j_d \end{bmatrix}, \quad \bar{I}_1 = \begin{bmatrix} 1 \\ 0 \\ 0 \end{bmatrix}, \quad \tilde{I}_1(z) = \begin{bmatrix} \dfrac{1}{R+z} \\ 0 \\ 0 \end{bmatrix},$$

$$w_{0_d} = \begin{bmatrix} w_{0,\theta}/R \\ w_{0,x} \end{bmatrix}, \quad w_{0_{dd}} = \begin{bmatrix} w_{0,\theta\theta}/R^2 \\ w_{0,\theta x}/R \\ w_{0,x\theta}/R \\ w_{0,xx} \end{bmatrix}, \quad u_{0_d} = \begin{bmatrix} u_{0_\theta,\theta}/R \\ u_{0_\theta,x} \\ u_{0_x,\theta}/R \\ u_{0_x,x} \end{bmatrix}, \quad \psi_{0_d} = \begin{bmatrix} \psi_{0_\theta,\theta}/R \\ \psi_{0_\theta,x} \\ \psi_{0_x,\theta}/R \\ \psi_{0_x,x} \end{bmatrix}, \tag{39}$$

$$\phi^j_d = \begin{bmatrix} \phi^j_{,\theta}/R \\ \phi^j_{,x} \end{bmatrix}, \quad \phi^j_{0_{dd}} = \begin{bmatrix} \phi^j_{,\theta\theta}/R^2 \\ \phi^j_{,\theta x}/R \\ \phi^j_{,x\theta}/R \\ \phi^j_{,xx} \end{bmatrix}, \quad T^l_d = \begin{bmatrix} T^l_{,\theta}/R \\ T^l_{,x} \end{bmatrix}, \quad T^l_{0_{dd}} = \begin{bmatrix} T^l_{,\theta\theta}/R^2 \\ T^l_{,\theta x}/R \\ T^l_{,x\theta}/R \\ T^l_{,xx} \end{bmatrix}.$$

4. Equilibrium equations and boundary conditions

The variational principle for the piezoelectric shell is given by

$$\int_V (\sigma_{ij}\delta\varepsilon_{ij} + D_i\delta\phi_{,i})\,dV - \int_\Gamma (T_i^n\delta u_i + D_n\delta\phi)\,d\Gamma - \sum_{i=1}^{n_\phi}\int_{A^{j_i}} q_{j_i}\delta\phi^{j_i}\,dA^{j_i} = 0 \tag{40}$$

(see [Tiersten 1969]), where V and Γ denote the volume and the surface area of the shell; A^{j_i} is an internal surface area at $z = z_\phi^{j_i}$ where ϕ^{j_i} is prescribed and q_{j_i} is the jump in electric displacement D_z at this interface; the total number of such prescribed potentials is $\bar{n}_\phi$; and D_n, T_i^n denote the electric displacement vector and surface traction vector on a surface with outward normal vector $\bar{n}$.

Let p_z^1 and p_z^2 be the normal forces per unit area, and D_z^1 and D_z^2 be the surface charge density applied on the bottom and top surfaces of the shell. Using the notation

$$\langle \dots \rangle = \sum_{k=1}^{L}\int_{z_{k-1}^+}^{z_k^-} (\dots)\,dz$$

for integration across the thickness, the variational equation (40) for the laminated piezoelectric cylindrical shell panel of length a and span angle α can be expressed as

$$\begin{aligned}
\int_0^a\int_0^\alpha \Bigg(\Big\langle \Big(1+\frac{z}{R}\Big)\Big\{ &\sigma_\theta\delta\varepsilon_\theta + \sigma_x\delta\varepsilon_x + \tau_{\theta x}\delta\gamma_{\theta x} + \tau_{\theta z}\delta\gamma_{\theta z} + \tau_{xz}\delta\gamma_{xz} + \frac{D_\theta\delta\phi_{,\theta}}{R+z} + D_x\delta\phi_{,x} + D_z\delta\phi_{,z}\Big\}\Big\rangle \\
&- p_z^1\Big(1+\frac{z_0}{R}\Big)\delta w(x,\theta,z_0) + D_z^1\Big(1+\frac{z_0}{R}\Big)\delta\phi^1 \\
&- p_z^2\Big(1+\frac{z_L}{R}\Big)\delta w(x,\theta,z_L) - D_z^2\Big(1+\frac{z_L}{R}\Big)\delta\phi^{n_\phi} - q_{j_i}\Big(1+\frac{z_\phi^{j_i}}{R}\Big)\delta\phi^{j_i}\Bigg) R\,d\theta\,dx \\
&- \int_0^a \langle \sigma_\theta\delta u_\theta + \tau_{\theta x}\delta u_x + + \tau_{\theta z}\delta w + D_\theta\delta\phi\rangle\Big|_0^\alpha dx \\
&- \int_0^\alpha \Big\langle \Big(1+\frac{z}{R}\Big)(\tau_{\theta x}\delta u_\theta + \sigma_x\delta u_x + \tau_{xz}\delta w + D_x\delta\phi)\Big\rangle\Big|_0^a R\,d\theta = 0,
\end{aligned} \tag{41}$$

for all δu_0, δw_0, $\delta\psi_0$, and $\delta\phi^j$. This variational equation is expressed in terms of δu_0, δw_0, $\delta\psi_0$, and $\delta\phi^j$ to yield the governing equations of equilibrium for the shell and its variationally consistent boundary conditions.

Using (36), the strain energy terms in (41) can be expressed as

$$\left\langle\left(1+\frac{z}{R}\right)[\delta\varepsilon^{\mathrm{T}}\sigma+\delta\gamma^{\mathrm{T}}\tau]\right\rangle=\delta u_{0_d}^{\mathrm{T}}\hat{N}-\delta w_{0_{dd}}^{\mathrm{T}}M+\delta\psi_{0_d}^{\mathrm{T}}P+\delta\psi_{dd}^{j^{\mathrm{T}}}S^j+\frac{\delta w_0 N_\theta}{R}-\frac{\delta\phi^j\hat{S}_\theta^j}{R}+\delta\psi_0^{\mathrm{T}}Q+\delta\phi_d^{j^{\mathrm{T}}}\bar{Q}^j,$$

where

$$\begin{aligned}
\hat{N}&=\begin{bmatrix}N_\theta+M_\theta/R\\ N_{x\theta}+M_{x\theta}/R\\ N_{\theta x}\\ N_x\end{bmatrix}=\left\langle\left(1+\frac{z}{R}\right)\Phi^{0^{\mathrm{T}}}(z)\sigma\right\rangle, \qquad M=\begin{bmatrix}M_\theta\\ M_{x\theta}\\ M_{\theta x}\\ M_x\end{bmatrix}=\left\langle\left(1+\frac{z}{R}\right)\Phi^{\mathrm{T}}(z)\sigma\right\rangle,\\
P&=\begin{bmatrix}P_\theta\\ P_{x\theta}\\ P_{\theta x}\\ P_x\end{bmatrix}=\left\langle\left(1+\frac{z}{R}\right)\Phi^{k^{\mathrm{T}}}(z)\sigma\right\rangle, \qquad \text{and} \qquad S^j=\begin{bmatrix}S_\theta^j\\ S_{x\theta}^j\\ S_{\theta x}^j\\ S_x^j\end{bmatrix}=\left\langle\left(1+\frac{z}{R}\right)\Phi^{kj^{\mathrm{T}}}(z)\sigma\right\rangle
\end{aligned} \tag{42}$$

are stress resultants of the inplane stress components σ (and likewise $\hat{S}^j$, defined analogously), and

$$Q=\begin{bmatrix}Q_\theta\\ Q_x\end{bmatrix}=\left\langle\left(1+\frac{z}{R}\right)\Phi_0^{k^{\mathrm{T}}}(z)\tau\right\rangle \qquad \text{and} \qquad \bar{Q}^j=\begin{bmatrix}\bar{Q}_\theta^j\\ \bar{Q}_x^j\end{bmatrix}=\left\langle\left(1+\frac{z}{R}\right)\Phi_0^{kj^{\mathrm{T}}}(z)\tau\right\rangle \tag{43}$$

are the stress resultants of the shear stress τ. In these formulas $N_\theta=\langle\sigma_\theta\rangle$, $N_{x\theta}$, $N_{\theta x}=\langle\tau_{\theta x}\rangle$, and N_x are inplane force resultants; M_θ, $M_{x\theta}$, $M_{\theta x}$, and M_x are moment resultants; P_θ, $P_{x\theta}$, $P_{\theta x}$, P_x, $S_\theta^j=\langle\bar{\phi}^j(z)\sigma_\theta\rangle$, $S_{x\theta}^j$, $S_{\theta x}^j$, and S_x^j are higher-order moment resultants; and Q_θ, Q_x, $\bar{Q}_\theta^j$, and $\bar{Q}_x^j$ are higher-order transverse shear resultants.

The electrical enthalpy terms in (41) can be expressed as

$$\left\langle\left(1+\frac{z}{R}\right)\left(\frac{D_\theta\delta\phi_{,\theta}}{R+z}+D_x\delta\phi_{,x}+D_z\delta\phi_{,z}\right)\right\rangle=\frac{H_\theta^j\delta\phi_{,\theta}^j}{R}+H_x^j\delta\phi_{,x}^j+G^j\delta\phi^j, \tag{44}$$

where the shell electric resultants H_θ^j, H_x^j, and G^j of electric displacements D_θ, D_x, and D_z are defined by

$$H^j=\begin{bmatrix}H_\theta^j\\ H_x^j\end{bmatrix}=\begin{bmatrix}\langle\Psi_\phi^j(z)D_\theta\rangle\\ \left\langle\left(1+\frac{z}{R}\right)\Psi_\phi^j(z)D_x\right\rangle\end{bmatrix}=\left\langle\Psi_\phi^j(z)\begin{bmatrix}1 & 0\\ 0 & 1+\frac{z}{R}\end{bmatrix}D\right\rangle, \quad G^j=\left\langle\left(1+\frac{z}{R}\right)\Psi_{\phi,z}^j(z)D_z\right\rangle. \tag{45}$$

The electromechanical loading terms in (41) can be expressed as $-(F_3\delta w_0+F_6^j\delta\phi^j)$ where F_3 and F_6^j are the mechanical and electrical loads respectively, defined by

$$\begin{aligned}
F_3&=\left(1+\frac{z_0}{R}\right)p_z^1+\left(1+\frac{z_L}{R}\right)p_z^2.\\
F_6^j&=-\left(1+\frac{z_0}{R}\right)p_z^1\bar{\Psi}_\phi^j(z_0)-\left(1+\frac{z_L}{R}\right)p_z^2\bar{\Psi}_\phi^j(z_L)+\left(1+\frac{z_L}{R}\right)D_z^2\delta_{jn_\phi}-\left(1+\frac{z_0}{R}\right)D_z^1\delta_{j1}+\left(1+\frac{z_\phi^{j_i}}{R}\right)q_{j_i}\delta_{jj_i}.
\end{aligned} \tag{46}$$

The boundary terms in (41) are similarly expressed in terms of the stress and electric resultants and its area integral is expressed in terms of δu_{0_θ}, δu_{0_x}, δw_0, $\delta\psi_{0_\theta}$, $\delta\psi_{0_x}$, and $\delta\phi^j$ by applying Green's theorem, wherever required, to yield the following $5+n_\phi$ equations of equilibrium:

$$\begin{gathered}
\frac{N_{\theta,\theta}}{R}+\frac{M_{\theta,\theta}}{R^2}+N_{x\theta,x}+\frac{M_{x\theta,x}}{R}=0, \qquad \frac{M_{\theta,\theta\theta}}{R^2}+\frac{(M_{x\theta}+M_{\theta x})_{,x\theta}}{R}+M_{x,xx}-\frac{N_\theta}{R}+F_3=0,\\
N_{x,x}+\frac{N_{\theta x,\theta}}{R}=0, \qquad \frac{P_{\theta,\theta}}{R}+P_{x\theta,\theta}-Q_\theta=0, \qquad \frac{P_{\theta x,\theta}}{R}+P_{x,x}-Q_x=0,\\
\frac{\bar{Q}^j_{\theta,\theta}}{R}+\bar{Q}^j_{x,x}-\left(\frac{S^j_{\theta,\theta\theta}}{R^2}+\frac{S^j_{\theta x,\theta x}}{R}+\frac{S^j_{x\theta,x\theta}}{R}+S^j_{x,xx}\right)+\frac{H^j_{\theta,\theta}}{R}+H^j_{x,x}-G^j+\frac{\hat{S}^j_\theta}{R}+F^j_6=0,
\end{gathered} \tag{47}$$

and boundary conditions which consist of prescribed values of one of the factors of each of the following products at $\theta=0,\alpha$:

$$\begin{gathered}
u_{0_\theta}\left(N_\theta+\frac{M_\theta}{R}\right), \qquad u_{0_x}N_{\theta x}, \quad w_0\left(M_{x\theta,x}+\frac{M_{\theta,\theta}}{R}+M_{\theta x,x}\right), \qquad w_{0,\theta}M_\theta,\\
\psi_{0_\theta}P_\theta, \qquad \psi_{0_x}P_{\theta x}, \quad \phi^j\left(\bar{Q}^j_\theta+H^j_\theta-\frac{S^j_{\theta,\theta}}{R}-S^j_{x\theta,x}-S^j_{\theta x,x}\right), \qquad \phi^j_{,\theta}S^j_\theta,
\end{gathered} \tag{48}$$

and at $x=0,a$:

$$\begin{gathered}
u_{0_\theta}\left(N_{x\theta}+\frac{M_{x\theta}}{R}\right), \qquad u_{0_x}N_x, \quad w_0\left(M_{x,x}+\frac{M_{\theta x,\theta}}{R}+\frac{M_{x\theta,\theta}}{R}\right), \qquad w_{0,x}M_x,\\
\psi_{0_\theta}P_{x\theta}, \qquad \psi_{0_x}P_x, \quad \phi^j\left(\bar{Q}^j_x+H^j-\frac{S^j_{x\theta,\theta}}{R}-\frac{S^j_{\theta x,\theta}}{R}-S^j_{x,x}\right), \qquad \phi^j_{,x}S^j_x.
\end{gathered} \tag{49}$$

The first term of each product corresponds to the essential boundary condition and the second term corresponds to the natural boundary condition.

We now turn to the shell constitutive equations, which are the relations between shell stress resultants and electric displacement resultants defined in (42), (43) and (45) with the generalised shell mechanical strains and electric potential entities. They are obtained by substituting the expressions of σ, τ, D, and D_z from (1) into (42), (43) and (45):

$$\begin{aligned}
F_1&=\left[\hat{N}^{\mathrm{T}}\ \ M^{\mathrm{T}}\ \ P^{\mathrm{T}}\ \ S^{j^{\mathrm{T}}}\right]^{\mathrm{T}}=A\bar{\varepsilon}_1+\beta^{j'}\phi^{j'}+A^lT^l_{dd}+(\tilde{A}^l-\gamma^l)T^l+\hat{A}\bar{u}_2,\\
F_2&=\left[Q^{\mathrm{T}}\ \ \bar{Q}^{j^{\mathrm{T}}}\right]^{\mathrm{T}}=\bar{A}\bar{\varepsilon}_2+\bar{\beta}^{j'}\phi^{j'}_d+\bar{A}^lT^l_d,\\
\bar{F}_2&=\left[N_\theta/R\ \ \hat{S}^j_\theta/R\right]^{\mathrm{T}}=\hat{A}^{\mathrm{T}}\bar{\varepsilon}_1+\hat{A}^*\bar{u}_2+\hat{\beta}^{j'}\phi^{j'}+\hat{A}^lT^l_{dd}+(A^{*l}-\hat{\gamma}^l)T^l,\\
H^j&=\bar{\beta}^{j^{\mathrm{T}}}\bar{\varepsilon}_2-\bar{E}^{jj'}\phi^{j'}_d+\bar{\beta}^{jl}T^l_d, \qquad G^j=\beta^{j^{\mathrm{T}}}\bar{\varepsilon}_1+\hat{\beta}^{j^{\mathrm{T}}}\bar{u}_2-E^{jj'}\phi^{j'}+\beta^{jl}T^l_{dd}+(\tilde{\gamma}^{jl}+\gamma^{jl})T^l,
\end{aligned} \tag{50}$$

where A, $\bar{A}$, $\hat{A}$, and $\hat{A}^*$ are the shell stiffnesses; A^l, $\bar{A}^l$, and $\hat{A}^l$ are the shell thermomechanical coefficients; $\beta^{j'}$, $\bar{\beta}^{j'}$, and $\hat{\beta}^j$ are the shell electromechanical coupling matrices; β^{jl}, $\bar{\beta}^{jl}$, γ^l, $\hat{\gamma}^l$, $\tilde{A}^l$, A^{*l}, and $\tilde{\gamma}^{jl}$ are the shell electrothermal matrices; γ^{jl} is the shell pyroelectric matrix; and $E^{jj'}$ and $\bar{E}^{jj'}$ are the shell

dielectric matrices. These are defined in terms of material constants by

$$
\begin{aligned}
[A, A^l, \tilde{A}^l] &= \left\langle \left(1+\frac{z}{R}\right) f_3^{\mathrm{T}}(z)\bar{Q}[f_3(z), \bar{\Phi}^{kl}(z), \tilde{I}_1(z)\bar{\Psi}_T^l(z)] \right\rangle, \\
[\bar{A}, \bar{A}^l] &= \left\langle \left(1+\frac{z}{R}\right) f_4^{\mathrm{T}}(z)\hat{Q}[f_4(z), \bar{\Phi}_0^{kl}(z)] \right\rangle, \qquad \hat{A} = \left\langle \frac{f_3^{\mathrm{T}}(z)\bar{Q}_1^{\mathrm{T}} f_2(z)}{R} \right\rangle, \\
\hat{A}^* &= \left\langle \frac{f_2^{\mathrm{T}}(z)\bar{Q}_{11} f_2(z)}{R(R+z)} \right\rangle, \qquad A^{*l} = \left\langle \frac{f_2^{\mathrm{T}}(z)\bar{Q}_{11}\bar{\Psi}_T^l(z)}{R(R+z)} \right\rangle, \\
\hat{A}^l &= \left\langle \frac{f_2^{\mathrm{T}}(z)\bar{Q}_1\bar{\Phi}^{kl}(z)}{R} \right\rangle, \qquad \beta^{j'} = \left\langle \left(1+\frac{z}{R}\right) f_3^{\mathrm{T}}(z)\bar{e}_3^{\mathrm{T}}\Psi_{\phi,z}^{j'}(z) \right\rangle, \\
\bar{\beta}^{j'} &= \left\langle f_4^{\mathrm{T}}(z)\hat{e} I_z^*(z)\Psi_\phi^{j'}(z) \right\rangle, \qquad \hat{\beta}^{j'} = \left\langle \frac{f_2^{\mathrm{T}}(z)\bar{e}_{31}\Psi_{\phi,z}^{j}(z)}{R} \right\rangle, \\
\beta^{jl} &= \left\langle \left(1+\frac{z}{R}\right) \Psi_{\phi,z}^{j}(z)\bar{e}_3\bar{\Phi}^{kl}(z) \right\rangle, \qquad \bar{\beta}^{jl} = \left\langle I_z^*(z)\Psi_\phi^j(z)\hat{e}^{\mathrm{T}}\bar{\Phi}_0^{kl}(z) \right\rangle, \\
\gamma^{\,l} &= \left\langle \left(1+\frac{z}{R}\right) f_3^{\mathrm{T}}(z)\bar{\beta}\Psi_T^l(z) \right\rangle, \qquad \hat{\gamma}^{\,l} = \left\langle \frac{f_2^{\mathrm{T}}(z)\bar{\beta}_1\Psi_T^l(z)}{R} \right\rangle, \\
E^{jj'} &= \left\langle \left(1+\frac{z}{R}\right) \bar{\eta}_{33}\Psi_{\phi,z}^{j}(z)\Psi_{\phi,z}^{j'}(z) \right\rangle, \qquad \bar{E}^{jj'} = \left\langle I_z^*(z)\hat{\eta}C_1(z)\Psi_\phi^j(z)\Psi_\phi^{j'}(z) \right\rangle, \\
\gamma^{\,jl} &= \left\langle \left(1+\frac{z}{R}\right) \bar{p}_3\Psi_{\phi,z}^{j}(z)\Psi_T^l(z) \right\rangle, \qquad \tilde{\gamma}^{\,jl} = \left\langle \frac{\Psi_{\phi,z}^{j}(z)\bar{e}_{31}\bar{\Psi}_T^l(z)}{R} \right\rangle,
\end{aligned}
\tag{51}
$$

with

$$
\bar{Q}_1 = \begin{bmatrix} Q_{11} & Q_{12} & Q_{16} \end{bmatrix}, \qquad I_z^*(z) = \begin{bmatrix} 1 & 0 \\ 0 & 1+\dfrac{z}{R} \end{bmatrix}. \tag{52}
$$

5. Angle-ply shell under cylindrical bending

Consider an angle-ply circular cylindrical shell panel of infinite length for which the applied thermoelectromechanical loading and hence all response entities are independent of x. The governing field equations, the boundary conditions, and the shell constitutive equations for such a shell under cylindrical bending are obtained by setting $(\,)_{,x} = 0$ in (47), (48), (49), and (50) for general bending of shell. Substituting the expressions of the resultants into the governing equations for the case of cylindrical bending yields the following coupled electromechanical equations in terms of the primary variables $u_{0\theta}$, u_{0x}, w_0, $\psi_{0\theta}$, ψ_{0x}, and ϕ^j:

$$
L\bar{U} = \bar{P}, \tag{53}
$$

where

$$
\begin{aligned}
\bar{U} &= \begin{bmatrix} u_{0\theta} & u_{0x} & w_0 & \psi_{0\theta} & \psi_{0x} & \phi^1 & \phi^2 & \dots & \phi^{n_\phi} \end{bmatrix}^{\mathrm{T}}, \\
\bar{P} &= \begin{bmatrix} P_1 & P_2 & P_3 & P_4 & P_5 & P_6^1 & P_6^2 & \dots & P_6^{n_\phi} \end{bmatrix}^{\mathrm{T}}.
\end{aligned}
\tag{54}
$$

L is a symmetric matrix of linear differential operators in θ, whose elements are given by

$$L_{11}=\frac{-A_{11}(),_{\theta\theta}}{R^2},\qquad L_{12}=\frac{-A_{13}(),_{\theta\theta}}{R^2},\qquad L_{13}=\frac{A_{15}(),_{\theta\theta\theta}}{R^3}-\frac{\hat{A}_{11}(),_{\theta}}{R},\qquad L_{14}=\frac{-A_{19}(),_{\theta\theta}}{R^2},$$

$$L_{15}=\frac{-A_{1,11}(),_{\theta\theta}}{R^2},\qquad L_{1,5+j'}=\frac{-A^{j'}_{1,13}(),_{\theta\theta\theta}}{R^3}+\frac{(\hat{A}^{j'}_{12}-\beta^{j'}_{1})(),_{\theta}}{R},\qquad L_{22}=\frac{-A_{33}(),_{\theta\theta}}{R^2},$$

$$L_{23}=\frac{A_{35}(),_{\theta\theta\theta}}{R^3}-\frac{\hat{A}_{31}(),_{\theta}}{R},\qquad L_{24}=\frac{-A_{39}(),_{\theta\theta}}{R^2},\qquad L_{25}=\frac{-A_{3,11}(),_{\theta\theta}}{R^2},$$

$$L_{2,5+j'}=\frac{-A^{j'}_{3,13}(),_{\theta\theta\theta}}{R^3}+\frac{(\hat{A}^{j'}_{32}-\beta^{j'}_{3})(),_{\theta}}{R},\qquad L_{33}=-\hat{A}^{*}_{11}-\frac{A_{55}(),_{\theta\theta\theta\theta}}{R^4}+\frac{(\bar{A}_{11}+2\hat{A}_{51})(),_{\theta\theta}}{R^2},$$

$$L_{34}=\frac{A_{59}(),_{\theta\theta\theta}}{R^3}+\frac{(\bar{A}_{13}-\hat{A}_{91})(),_{\theta}}{R},\qquad L_{35}=\frac{A_{5,11}(),_{\theta\theta\theta}}{R^3}+\frac{(\bar{A}_{14}-\hat{A}_{11,1})(),_{\theta}}{R},$$

$$L_{3,5+j'}=\frac{(\beta^{j'}_{5}-\hat{A}^{j'}_{52}-\hat{A}^{j'}_{13,1}+\bar{A}^{j'}_{15}+\bar{\beta}^{j'}_{11})(),_{\theta\theta}}{R^2}+\frac{A^{j'}_{5,13}(),_{\theta\theta\theta\theta}}{R^4}+\hat{A}^{*j'}_{12}-\hat{\beta}^{j'}_{1},\quad L_{44}=\bar{A}_{33}-\frac{A_{99}(),_{\theta\theta}}{R^2},$$

$$L_{45}=\bar{A}_{34}-\frac{A_{9,11}(),_{\theta\theta}}{R^2},\qquad L_{4,5+j'}=\frac{-A^{j'}_{9,13}(),_{\theta\theta\theta}}{R^3}+\frac{(\bar{A}^{j'}_{35}+\bar{\beta}^{j'}_{31}-\beta^{j'}_{9}+\hat{A}^{j'}_{92})(),_{\theta}}{R},$$

$$L_{55}=\bar{A}_{44}-\frac{A_{11,11}(),_{\theta\theta}}{R^2},\qquad L_{5,5+j'}=\frac{-A^{j'}_{11,13}(),_{\theta\theta\theta}}{R^3}+\frac{(\bar{A}^{j'}_{45}+\bar{\beta}^{j'}_{41}-\beta^{j'}_{11}+\hat{A}^{j'}_{11,2})(),_{\theta}}{R},$$

$$L_{5+j,5+j'}=\frac{(\bar{A}^{jj'}_{55}-\beta^{jj'}_{13}-\beta^{j'j}_{13}+\bar{\beta}^{jj'}_{51}+\bar{\beta}^{j'j}_{51}-\bar{E}^{jj'}_{11}+\hat{A}^{jj'}_{13,2}+\hat{A}^{j'j}_{13,2})(),_{\theta\theta}}{R^2}-\frac{A^{jj'}_{13,13}(),_{\theta\theta\theta\theta}}{R^4}$$
$$+E^{jj'}-\hat{A}^{*jj'}_{22}+\hat{\beta}^{jj'}_{2}+\hat{\beta}^{j'j}_{2},$$

for $(j,\, j')=1,\ldots n_{\phi}$. The elements of the load vector $\bar{P}$ are

$$P_1=\frac{A^{l}_{11}T^{l}_{,\theta\theta\theta}}{R^3}+\frac{(\tilde{A}^{l}_{1}-\gamma^{l}_{1})T^{l}_{,\theta}}{R},\qquad P_2=\frac{A^{l}_{31}T^{l}_{,\theta\theta\theta}}{R^3}+\frac{(\tilde{A}^{l}_{3}-\gamma^{l}_{3})T^{l}_{,\theta}}{R},$$

$$P_3=\frac{(\gamma^{l}_{5}-\tilde{A}^{l}_{5}+\hat{A}^{l}_{11}-\bar{A}^{l}_{11})T^{l}_{,\theta\theta}}{R^2}-F_3-\frac{A^{l}_{51}T^{l}_{,\theta\theta\theta\theta}}{R^4}+(A^{*l}_{1}-\hat{\gamma}^{l}_{1})T^{l},$$

$$P_4=\frac{A^{l}_{91}T^{l}_{,\theta\theta\theta}}{R^3}-\frac{(\gamma^{l}_{9}-\tilde{A}^{l}_{9}+\bar{A}^{l}_{31})T^{l}_{,\theta}}{R},\qquad P_5=\frac{A^{l}_{11,1}T^{l}_{,\theta\theta\theta}}{R^3}-\frac{(\gamma^{l}_{11}-\tilde{A}^{l}_{11}+\bar{A}^{l}_{41})T^{l}_{,\theta}}{R},$$

$$P^{j}_{6}=-F^{j}_{6}-\frac{(\bar{A}^{jl}_{51}+\bar{\beta}^{jl}_{11}-\beta^{jl}_{1}+\gamma^{jl}_{13}-\tilde{A}^{jl}_{13})T^{l}_{,\theta\theta}}{R^2}+(\gamma^{jl}+\tilde{\gamma}^{jl})T^{l}+\frac{A^{jl}_{13,1}T^{l}_{,\theta\theta\theta\theta}}{R^4}+(\hat{\gamma}^{jl}_{2}-A^{*jl}_{2})T^{l}-\frac{\hat{A}^{jl}_{21}T^{l}_{,\theta\theta}}{R^2}.$$

To assess the accuracy of the theories developed herein, a Fourier series solution is obtained for simply supported angle-ply shell panels of span angle α for the following boundary conditions at $\theta=0,\,\alpha$:

$$N_{\theta}+\frac{M_{\theta}}{R}=0,\quad N_{\theta x}=0,\quad \omega_0=0,\quad M_{\theta}=0,\quad P_{\theta}=0,\quad P_{\theta x}=0,\quad \phi^{j}=0,\quad S^{j}_{\theta}=0,\qquad (55)$$

for $j = 1, \ldots, n_\phi$. The load parameters and the solution are expanded in Fourier series, satisfying the boundary conditions, as:

$$(u_{0_\theta}, u_{0_x}, \psi_{0_\theta}, \psi_{0_x}, Q_x, Q_\theta, \bar{Q}^j_\theta, H^j_\theta) = \sum_{m=1}^{\infty} (u_{0_\theta}, u_{0_x}, \psi_{0_\theta}, \psi_{0_x}, Q_x, Q_\theta, \bar{Q}^j_\theta, H^j_\theta)_m \cos(\bar{m}\theta),$$

$$(w_0, \phi^j, N_\theta, M_\theta, N_{\theta x}, P_\theta, P_{\theta x}, S^j_\theta, G^j, \hat{S}^j_\theta) = \sum_{m=1}^{\infty} (w_0, \phi^j, N_\theta, M_\theta, N_{\theta x}, P_\theta, P_{\theta x}, S^j_\theta, G^j, \hat{S}^j_\theta)_m \sin(\bar{m}\theta),$$

$$(p_i, \phi_i, D_i, T_i, \Phi_i, q_i) = \sum_{m=1}^{\infty} (p_i, \phi_i, D_i, T_i, \Phi_i, q_i)_m \sin(\bar{m}\theta),$$

with $\bar{m} = \dfrac{m\pi}{\alpha}$. Substituting these in (53) yields for the m-th Fourier component

$$K\bar{U}^m = \bar{P}^m. \tag{56}$$

$\bar{U}$ is partitioned into a set of five mechanical displacement variables U, a set of unknown output voltages Φ_s at z^j_ϕ where ϕ is not prescribed, and a set of known input actuation voltages Φ_a at the actuated surfaces. $\bar{P}$ is also partitioned accordingly. Equation (56) is then solved for the unknown variables U and Φ_s. The transverse shear stresses τ and normal stress σ_z are obtained by integrating the 3D equations of equilibrium.

6. Assessment of the theories

The IZIGT and ITOT developed herein are assessed for accuracy by comparison with the exact 3D piezothermoelasticity solution by Dumir et al. [1997] for simply supported hybrid angle-ply cylindrical shell panels in cylindrical bending. The exact 3D results for various laminate configurations have been generated using the computer program developed by the same authors for their numerical study.

Three laminate configurations (a), (b), and (c) as shown in Figure 2 are considered for the assessment. The orientation of the principal material direction is mentioned with respect to θ-axis. Laminate (a), which has been devised as a benchmark test case, has an elastic substrate of five plies of materials 1/2/3/1/3 having highly inhomogeneous properties for tensile and shear stiffnesses, coefficients of thermal expansion, as well as thermal conductivities. A piezoelectric layer of PZT-5A is bonded to the top (outer) surface of the substrate. Laminate (b) has a four-ply graphite-epoxy composite substrate of material 4 and

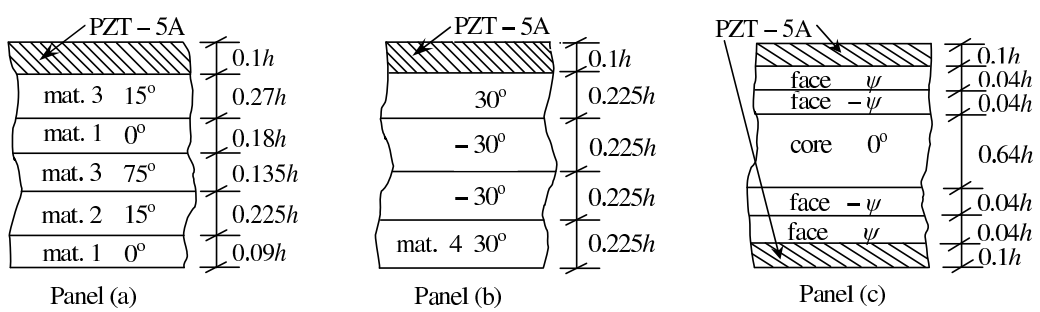

Figure 2. Configurations of hybrid cylindrical panels.

a PZT-5A layer bonded to its top surface. Laminate (c) has a sandwich substrate with two-ply composite faces and a soft core, and two layers of PZT-5A bonded to its top and bottom surfaces. The span angle is taken as 120° and the fibre orientation angle for the sandwich panel (c) is taken as 30° unless otherwise mentioned. The interfaces between the substrates and the piezoelectric layers are grounded. The outer surfaces of all the panels are in a close circuit condition with the prescribed electric potentials, while the inner surface of panel (c) is in an open circuit condition with the prescribed charge density and unknown electric potential.

Material constants and thermal conductivities, along with properties of PZT-5A, are given in Table 1.

The following mechanical, potential, and thermal load cases are considered:

(1) Pressure load $p_z^2 = -p_0 \sin(\pi\theta/\alpha)$ applied on the top surface.

(2) Potential load $\phi^n{}^{\phi} = \phi_0 \sin(\pi\theta/\alpha)$ applied on the top surface.

(3) Thermal load $T(\theta, -h/2) = T_0 \sin(\pi\theta/\alpha)$, $T(\theta, h/2) = 0$.

The results for the three load cases are nondimensionalised as shown in Table 2.

The 3D thermal problem is solved as in [Dumir et al. 1997], by analytically solving the heat conduction equation for all layers and satisfying the thermal boundary conditions and the continuity conditions at layer interfaces for temperature and heat flow. The distributions of temperature across the thickness for load case 3 is shown in Figure 3. It has been found from convergence studies that converged results

	Y_1	Y_2	Y_3	G_{23}	G_{13}	G_{12}
Material 1	6.9	6.9	6.9	2.76	2.76	2.76
Material 2	224.25	6.9	6.9	1.38	56.58	56.58
Material 3	172.5	6.9	6.9	1.38	3.45	3.45
Material 4	181.0	10.3	10.3	2.87	7.17	7.17
Face	131.1	6.9	6.9	2.3322	3.588	3.588
Core	2.208×10^{-4}	2.001×10^{-4}	2.76	0.4554	0.5451	0.01656
PZT-5A	61.0	61.0	53.2	21.1	21.1	22.6

	ν_{12}	ν_{13}	ν_{23}	α_1	α_2	α_3	k_1	k_2	k_3
Material 1	0.25	0.25	0.25	35.6	35.6	35.6	0.12	0.12	0.12
Material 2	0.25	0.25	0.25	0.25	35.6	35.6	7.2	1.44	1.44
Material 3	0.25	0.25	0.25	0.57	35.6	35.6	1.92	0.96	0.96
Material 4	0.28	0.28	0.33	0.02	22.5	22.5	1.5	0.5	0.5
Face	0.32	0.32	0.49	0.0225	22.5	22.5	1.5	0.5	0.5
Core	0.99	3×10^{-5}	3×10^{-5}	30.6	30.6	30.6	3.0	3.0	3.0
PZT-5A	0.35	0.38	0.38	1.5	1.5	2.0	1.8	1.8	1.8

	d_{31}	d_{32}	d_{33}	d_{24}	d_{15}	η_{11}	η_{22}	η_{33}	p_3
PZT-5A	−171	−171	374	584	584	15.3	15.3	15.0	0.0007

Table 1. Material constants Y_1, Y_2, Y_3, G_{23}, G_{13}, G_{12} (GPa); ν_{12}, ν_{13}, ν_{23}; α_1, α_2, α_3 ($10^{-6}\,\mathrm{K}^{-1}$); and thermal conductivities k_1, k_2, k_3 (W/m K). Other properties of PZT-5A d_{31}, d_{32}, d_{33}, d_{24}, d_{15} (pm/V); η_{11}, η_{22}, η_{33} (nF/m); and p_3 ($\mathrm{C/m^2\,K}$).

Pressure load case:
$$(\bar{u}_\theta, \bar{w}) = (u_\theta, w)\frac{Y_0}{hS^4 p_0}, \qquad \bar{D}_z = \frac{D_z}{10S^2 p_0 d_0},$$
$$(\bar{\sigma}_\theta, \bar{\sigma}_x, \bar{\sigma}_z, \bar{\tau}_{\theta x}, \bar{\tau}_{xz}, \bar{\tau}_{\theta z}) = \left(\frac{\sigma_\theta}{S}, \frac{\sigma_x}{S}, \sigma_z, \frac{\tau_{\theta x}}{S}, \tau_{xz}, \tau_{\theta z}\right)\frac{1}{10Sp_0}.$$

Potential load case:
$$(\bar{u}_\theta, \bar{w}) = \frac{(u_\theta, w)}{10S^2\phi_0 d_0}, \qquad \bar{D}_z = \frac{D_z h}{1000\phi_0 d_0^2 Y_0},$$
$$(\bar{\sigma}_\theta, \bar{\sigma}_x, \bar{\sigma}_z, \bar{\tau}_{\theta x}, \bar{\tau}_{xz}, \bar{\tau}_{\theta z}) = (\sigma_\theta, \sigma_x, \sigma_z S, \tau_{\theta x}, \tau_{xz} S, \tau_{\theta z} S)\frac{h}{10\phi_0 d_0 Y_0}.$$

Thermal load case:
$$(\bar{u}_\theta, \bar{w}) = \frac{10(u_\theta, w)}{hS^2\alpha_0 T_0}, \quad \bar{D}_z = \frac{D_z}{\alpha_0 T_0 Y_0 d_0}, \quad \bar{\phi} = \frac{1000\phi d_0}{\alpha_0 T_0 h},$$
$$(\bar{\sigma}_\theta, \bar{\sigma}_x, \bar{\sigma}_z, \bar{\tau}_{\theta x}, \bar{\tau}_{xz}, \bar{\tau}_{\theta z}) = (10\sigma_\theta, \sigma_x, 100\sigma_z S, \tau_{\theta x}, S\tau_{xz}, S\tau_{\theta z})\frac{1}{\alpha_0 T_0 Y_0}.$$

Table 2. Nondimensional magnitudes in the loading cases considered. Parameters in the formulas: $S = R/h$, $Y_0 = 6.9$ GPa for panels (a) and (c), $Y_0 = 10.3$ GPa for panel (b); $\alpha_0 = 35.6 \times 10^{-6}$ K^{-1} for panel (a), $\alpha_0 = 22.5 \times 10^{-6}$ K^{-1} for panels (b) and (c); and $d_0 = 374 \times 10^{-12}$ pm/V for all panels.

are obtained by approximating the exact temperature distributions across the thickness by the present sublayerwise linear distribution with 8 equal sublayers in the core of sandwich panel and 4 equal sublayers for all other laminas. For the distribution of electric potential, converged results are obtained by dividing each piezoelectric layer into 4 equal sublayers.

The exact 3D results and the percent errors in the results of the present 2D theories IZIGT and ITOT for displacements, predominant inplane normal stresses σ^e in the elastic substrate and σ^p in the piezoelectric layer, shear stresses, D_z and ϕ at typical points across the thickness, where they are large, are given in Tables 3–5 for panels (a), (b), and (c) for the pressure and potential load cases. The z-locations of the entities are mentioned within brackets. In order to investigate the influence of the thermoelectric

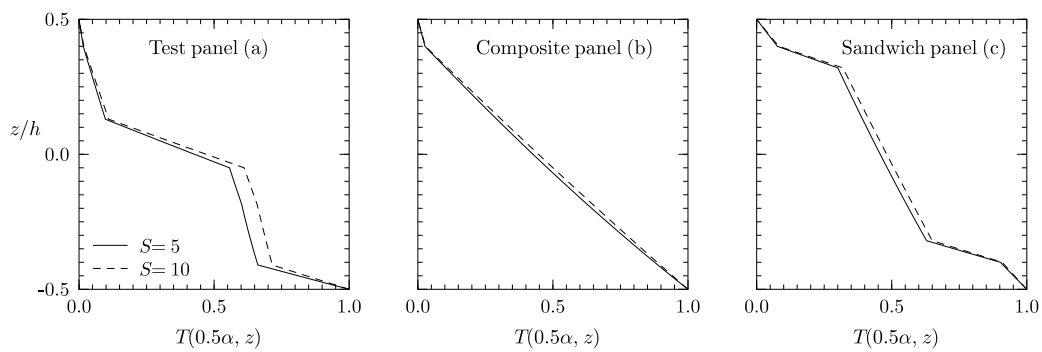

Figure 3. Temperature distributions in hybrid angle-ply cylindrical panels (a), (b), and (c).

	Load case 1				Load case 2					
S	Entity	Exact	IZIGT	ITOT	Entity	Exact	IZIGT	ZIGT	ITOT	TOT
5	$\bar{u}_\theta$	–0.57137	–4.56	–23.8	$\bar{u}_\theta$	0.13464	–2.60	–3.76	–5.63	–7.53
10	$(-0.5h)$	–0.40342	–1.62	–8.07	$(-0.5h)$	0.12403	–0.69	–1.39	–1.55	–2.46
20		–0.35424	–0.49	–2.27		0.12020	–0.16	–0.54	–0.39	–0.83
5	$\bar{w}$	–0.77787	–4.57	–24.7	$\bar{w}$	0.18944	–2.58	–3.71	–5.66	–7.55
10	(0)	–0.57234	–1.66	–8.30	(0)	0.18020	–0.69	–1.39	–1.56	–2.47
20		–0.51595	–0.51	–2.31		0.17744	–0.16	–0.54	–0.39	–0.83
5	$\bar{\sigma}_\theta^e$	0.98562	–0.10	–8.05	$\bar{\sigma}_\theta^e$	2.9186	–3.63	–4.40	–4.02	–5.22
10	$(-0.41h^+)$	0.84048	0.10	–2.00	$(0.4h^-)$	2.8458	–0.82	–1.41	–0.93	–1.64
20		0.78939	0.10	–0.43		2.8290	–0.12	–0.47	–0.15	–0.53
5	$\bar{\sigma}_\theta^p$	–0.35624	–3.83	–9.47	$\bar{\sigma}_x^p$	–5.7276	1.29	1.07	1.35	1.17
10	$(0.5h)$	–0.33133	–1.23	–2.85	$(0.4h^+)$	–5.7419	0.56	0.47	0.58	0.49
20		–0.32473	–0.45	–0.87		–5.7440	0.24	0.20	0.25	0.20
5	$\bar{\tau}_{\theta x}$	–0.14333	–3.48	–3.23	$\bar{\tau}_{\theta x}$	0.69887	–3.15	–3.86	–3.27	–4.44
10	$(0.4h^-)$	–0.13794	–1.14	–1.10	$(0.4h^-)$	0.68701	–0.48	–1.06	–0.51	–1.21
20		–0.13588	–0.40	–0.39		0.68492	0.07	–0.28	0.07	–0.32
5	$\bar{\tau}_{\theta z}$	–0.20590	0.72	2.35	$\bar{\tau}_{\theta z}$	0.20268	4.78	2.50	5.40	3.42
10	$(-0.05h)$	–0.19841	0.26	0.65	$(-0.21h)$	0.20421	1.67	0.66	1.84	0.91
20		–0.19363	0.10	0.20		0.20360	0.65	0.17	0.69	0.24
5	$\bar{D}_z$	0.18698	–0.64	–4.18	$\bar{D}_z$	–0.19026	–0.66	0.18	–0.74	0.08
10	$(0.5h)$	0.17955	0.42	–0.57	$(0.5h)$	–0.19101	–0.27	0.15	–0.29	0.13
20		0.17727	0.74	0.48		–0.19154	–0.11	0.10	–0.11	0.09

Table 3. Exact 3D results and percent errors of 2D theories for hybrid test panel (a) under load cases 1 and 2.

transverse normal strain, the results for the potential load case and the thermal load case (presented later) are also compared with the particular cases of the present theories wherein w is considered uniform across the thickness. The latter theories are referred to herein as the ZIGT and TOT. It is observed from these tables that the IZIGT yields accurate results for all response entities for both pressure and electric potential load cases even for thick hybrid panels with $S = 5$, having highly inhomogeneous lay-up. The ITOT with the same number of unknowns yields far inferior results with large error in the deflection and predominant inplane stress for the inhomogeneous test case and the sandwich panel under pressure loading. For the potential load case, the ITOT is quite accurate although inferior to IZIGT. For this load case, the IZIGT and ITOT are in general superior to their respective counterparts the ZIGT and TOT with uniform deflection approximation. The improvement is not restricted to w only, but holds well also for u_θ, σ_θ, and $\tau_{\theta x}$. Similar results for the thermal load case are presented in Tables 6 and 7 for hybrid cylindrical panels (a), (b), and (c). It is revealed from these results that inclusion of layerwise terms in the approximation of inplane displacements has far less effect on the results than the incorporation of the

	Load case 1				Load case 2					
S	Entity	Exact	IZIGT	ITOT	Entity	Exact	IZIGT	ZIGT	ITOT	TOT
5	$\bar{u}_\theta$	–0.79418	–2.81	–4.62	$\bar{u}_\theta$	0.14747	–0.91	–2.14	–1.80	–3.07
10	$(-0.5h)$	–0.62329	–0.86	–1.41	$(-0.5h)$	0.13644	–0.07	–0.78	–0.31	–1.05
20		–0.56802	–0.24	–0.39		0.13229	0.08	–0.30	0.02	–0.37
5	$\bar{w}$	–1.0772	–2.98	–4.81	$\bar{w}$	0.20551	–1.15	–2.30	–2.08	–3.31
10	(0)	–0.88373	–0.92	–1.47	(0)	0.19697	–0.10	–0.81	–0.36	–1.08
20		–0.82736	–0.26	–0.40		0.19462	0.07	–0.31	0.01	–0.38
5	$\bar{\sigma}_\theta^e$	0.62386	0.08	–0.63	$\bar{\sigma}_\theta^e$	1.5160	–1.75	–2.76	–2.14	–3.42
10	$(-0.5h)$	0.56103	0.06	–0.12	$(0.4h^-)$	1.5042	–0.31	–0.97	–0.41	–1.14
20		0.53462	0.03	–0.01		1.5028	0.00	–0.37	–0.03	–0.42
5	$\bar{\sigma}_\theta^p$	–0.37858	–2.22	–2.84	$\bar{\sigma}_x^p$	–3.8409	1.15	2.62	1.35	1.16
10	$(0.5h)$	–0.35979	–0.57	–0.75	$(0.4h^+)$	–3.8496	0.51	0.41	0.57	0.47
20		–0.35532	–0.20	–0.24		–3.8504	0.22	0.17	0.23	0.19
5	$\bar{\tau}_{\theta x}$	0.30147	0.15	–0.19	$\bar{\tau}_{\theta x}$	0.73238	–0.35	–1.41	0.05	–1.29
10	$(-0.5h)$	0.27576	0.10	0.02	$(0.4h^-)$	0.73872	0.38	–0.29	0.49	–0.26
20		0.26415	0.06	0.03		0.74212	0.34	–0.04	0.36	–0.03
5	$\bar{\tau}_{\theta z}$	–0.20207	0.26	0.11	$\bar{\tau}_{\theta z}$	–0.43799	1.75	0.04	2.66	0.99
10	(0)	–0.19365	0.05	0.01	$(0.4h)$	–0.45551	0.65	–0.18	0.90	0.08
20		–0.18926	0.00	0.00		–0.46292	0.27	–0.14	0.33	–0.08
5	$\bar{D}_z$	0.20302	0.66	0.33	$\bar{D}_z$	–0.12744	–0.57	0.26	–0.71	0.11
10	$(0.5h)$	0.19631	0.97	0.87	$(0.5h)$	–0.12797	–0.24	0.18	–0.28	0.14
20		0.19445	0.95	0.93		–0.12834	–0.10	0.12	–0.11	0.11

Table 4. Exact 3D results and percent errors of 2D theories for hybrid composite panel (b) under load cases 1 and 2.

layerwise terms in the transverse displacement. While the difference between the IZIGT and ITOT or between the ZIGT and TOT is not significant, the IZIGT and ITOT exhibit very significant improvement over their respective conventional counterparts the ZIGT and TOT, respectively. For the given load case, the reduction in error in the improved theories is over 70% for the deflection $\bar{w}$ and predominant inplane stress $\bar{\sigma}_\theta$. For the hybrid test and composite panels (a) and (b), the improved theories predict the deflection $\bar{w}$ with significant error (9–10%) even for thin panels with $S = 20$.

The through-the-thickness distributions of $\bar{u}_\theta$, $\bar{w}$, $\bar{\sigma}_\theta$, and $\bar{\tau}_{\theta z}$ predicted by the present 2D theories, the IZIGT and ITOT, are compared with the exact 3D solutions in Figures 4–8 for panels (a), (b), and (c). It is observed that even though the ITOT yields erroneous distributions for $\bar{u}_\theta$ and $\bar{w}$ for thick panels with $S = 5$, the distributions for $\bar{\sigma}_\theta$ and $\bar{\tau}_{\theta z}$ predicted by it are accurate for both load cases except for some error in the distributions in stiffer layers for $\bar{\sigma}_\theta$ for hybrid test panel (a) and sandwich panel (c) under pressure load. The IZIGT predicts more accurate distributions of these entities in all cases.

	Load case 1				Load case 2					
S	Entity	Exact	IZIGT	ITOT	Entity	Exact	IZIGT	ZIGT	ITOT	TOT
5	$\bar{u}_\theta$	–1.3080	–3.17	–19.9	$\bar{u}_\theta$	0.24821	–0.05	–1.58	–3.84	–4.94
10	$(-0.5h)$	–0.82100	–1.22	–7.61	$(-0.5h)$	0.23618	0.08	–0.73	–0.94	–1.64
20		–0.68738	–0.36	–2.22		0.23187	0.07	–0.34	–0.19	–0.58
5	$\bar{w}$	–1.8181	–3.08	–20.6	$\bar{w}$	0.36134	–0.02	–1.55	–3.85	–4.94
10	(0)	–1.1709	–1.25	–7.87	(0)	0.34907	0.08	–0.73	–0.94	–1.64
20		–1.0024	–0.37	–2.27		0.34524	0.07	–0.34	–0.19	–0.57
5	$\bar{\sigma}_\theta^e$	–0.54675	–0.02	1.63	$\bar{\sigma}_\theta^e$	3.8462	0.27	–1.23	0.60	–0.93
10	$(0.4h^-)$	–0.55914	–0.06	0.34	$(0.4h^-)$	3.8267	0.16	–0.63	0.26	–0.54
20		–0.56060	–0.04	0.06		3.8146	0.09	–0.31	0.12	–0.29
5	$\bar{\sigma}_\theta^p$	0.93850	–1.97	–8.23	$\bar{\sigma}_x^p$	–5.0918	0.53	0.66	0.47	0.61
10	$(-0.5h)$	0.77239	–0.93	–2.62	$(0.4h^+)$	–5.0862	0.22	0.29	0.20	0.28
20		0.71722	–0.60	–1.03		–5.0832	0.06	0.10	0.06	0.09
5	$\bar{\tau}_{\theta x}$	–0.28170	–0.66	1.01	$\bar{\tau}_{\theta x}$	1.9572	0.94	–0.58	1.34	–0.21
10	$(0.4h^-)$	–0.28768	–0.47	–0.07	$(0.4h^-)$	1.9543	0.50	–0.29	0.62	–0.18
20		–0.28794	–0.27	–0.17		1.9515	0.26	–0.14	0.29	–0.11
5	$\bar{\tau}_{\theta z}$	–0.17733	0.12	0.84	$\bar{\tau}_{\theta z}$	–0.37320	0.67	–0.84	0.98	–0.57
10	$(-0.32h)$	–0.16068	0.04	0.21	$(0.4h)$	–0.38334	0.28	–0.50	0.36	–0.42
20		–0.15238	0.01	0.06		–0.38824	0.12	–0.27	0.14	–0.25
5	$\bar{D}_z$	0.35811	1.94	–1.43	$\bar{D}_z$	–0.20263	–0.31	0.27	–0.34	0.24
10	$(0.5h)$	0.34826	1.17	0.26	$(0.5h)$	–0.20368	–0.13	0.17	–0.14	0.16
20		0.34504	0.95	0.71		–0.20426	–0.03	0.12	–0.04	0.11
5	$\bar{\phi}$	21.149	0.41	–3.70	$\bar{\phi}$	–0.010942	1.29	0.68	0.07	–1.08
10	$(-0.5h)$	18.686	0.31	–0.75	$(-0.5h)$	–0.010343	0.62	0.23	0.30	–0.22
20		17.727	0.18	–0.08		–0.010086	0.32	0.10	0.23	–0.02

Table 5. Exact 3D results and percent errors of 2D theories for hybrid sandwich panel (c) under load cases 1 and 2.

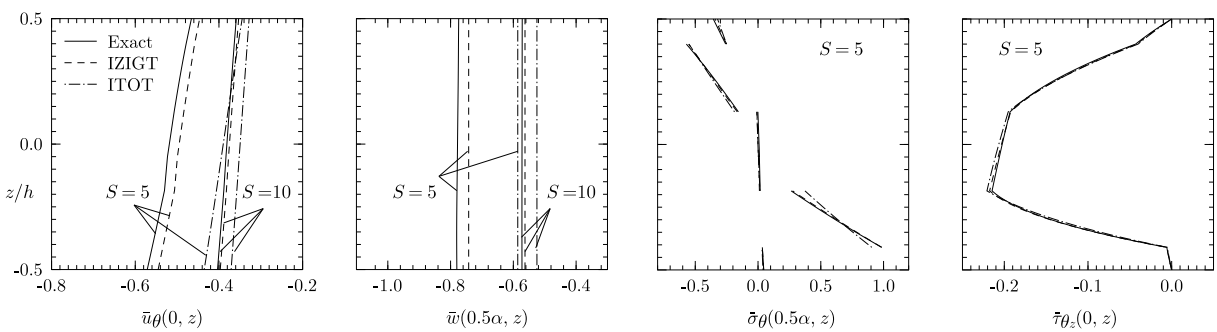

Figure 4. Through-the-thickness distributions of $\bar{u}_\theta$, $\bar{w}$, $\bar{\sigma}_\theta$, and $\bar{\tau}_{\theta z}$ for hybrid test panel (a) under load case 1.

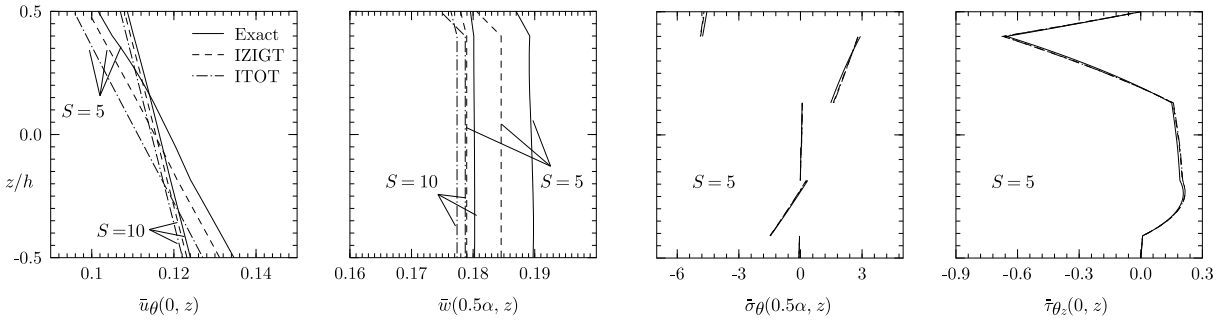

Figure 5. Through-the-thickness distributions of $\bar{u}_\theta$, $\bar{w}$, $\bar{\sigma}_\theta$, and $\bar{\tau}_{\theta z}$ for hybrid test panel (a) under load case 2.

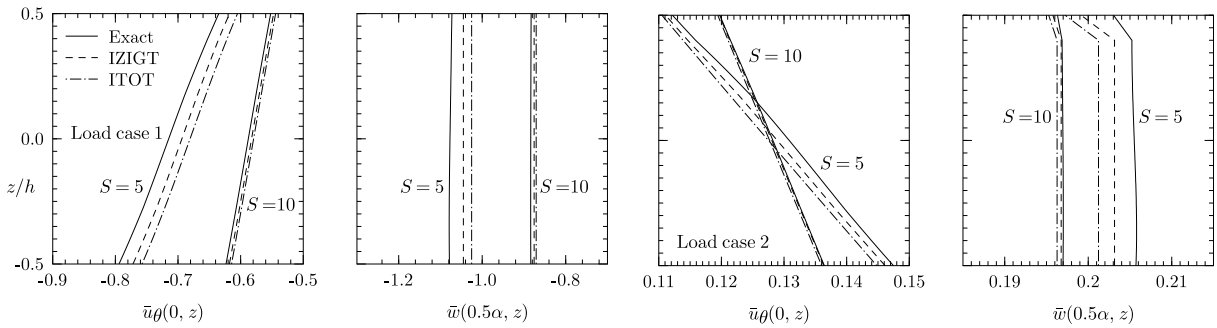

Figure 6. Through-the-thickness distributions of $\bar{u}_\theta$ and $\bar{w}$ for hybrid composite panel (b) under load cases 1 and 2.

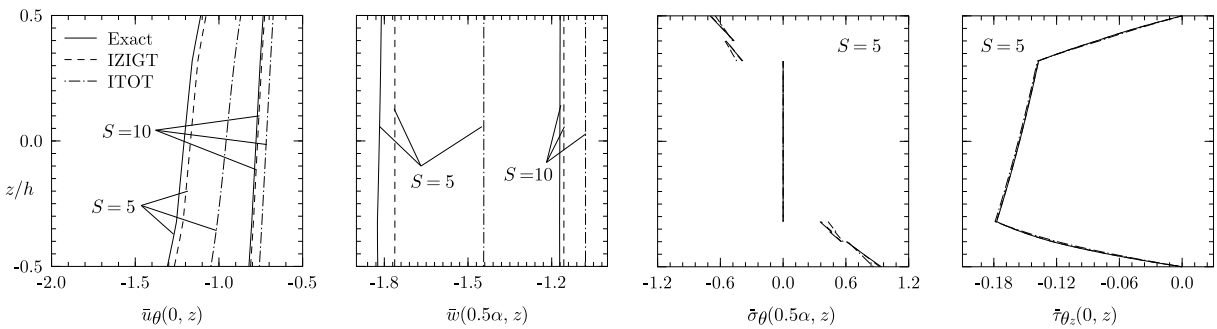

Figure 7. Through-the-thickness distributions of $\bar{u}_\theta$, $\bar{w}$, $\bar{\sigma}_\theta$, and $\bar{\tau}_{\theta z}$ for hybrid sandwich panel (c) under load case 1.

It is seen in Tables 6 and 7 that results of the IZIGT and ITOT do not show any significant difference for load case 3. To investigate the effect of inclusion of transverse normal strain, the through-the-thickness distributions of $\bar{u}_\theta$, $\bar{w}$, $\bar{\sigma}_\theta$, and $\bar{\tau}_{\theta z}$ obtained from the IZIGT and ZIGT, are compared with the exact 3D solutions in Figures 9–11 for panels (a), (b), and (c). The distributions of $\bar{\sigma}_z$ across the thickness, obtained by postprocessing from the 3D equilibrium equations, are shown in Figure 12. It is revealed that the assumption of uniform deflection in the conventional ZIGT causes erroneous distributions not only for the deflection $\bar{w}$, but also for inplane displacements and stresses for hybrid test and composite

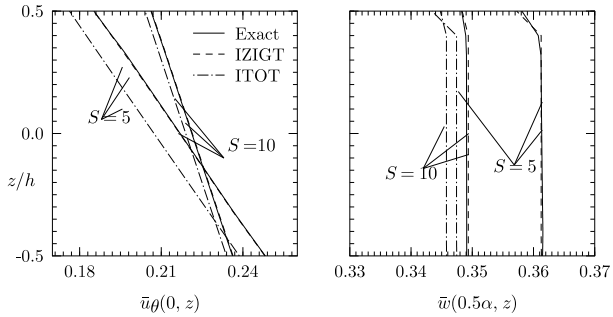

Figure 8. Through-the-thickness distributions of $\bar{u}_\theta$ and $\bar{w}$ for hybrid sandwich panel (c) under load case 2.

	Panel (a)					Panel (b)				
S	Entity	Exact	IZIGT	ZIGT	ITOT	TOT	Entity	Exact	IZIGT	ZIGT	ITOT	TOT
5	$\bar{u}_\theta$	–0.97476	–16.1	–62.5	–18.2	–64.5	$\bar{u}_\theta$	–1.0501	–17.1	–69.4	–17.6	–69.9
10	$(-0.5h)$	–0.63749	–12.3	–48.2	–13.2	–48.9	$(-0.5h)$	–0.63504	–13.5	–55.4	–13.7	–55.6
20		–0.46207	–8.33	–32.7	–8.65	–33.0		–0.43876	–9.53	–39.2	–9.60	–39.2
40		–0.37548	–5.06	–19.9	–5.16	–20.0		–0.34405	–6.00	–24.7	–6.02	–24.7
5	$\bar{w}$	–1.3929	–17.7	–68.0	–19.8	–70.0	$\bar{w}$	–1.5229	–18.0	–73.8	–18.5	–74.3
10	$(-0.5h)$	–0.91058	–13.3	–51.7	–14.2	–52.5	$(-0.5h)$	–0.91930	–14.2	–58.4	–14.4	–58.6
20		–0.66701	–8.80	–34.4	–9.13	–34.7		–0.63899	–9.90	–40.8	–9.98	–40.8
40		–0.54930	–5.23	–20.5	–5.33	–20.6		–0.50578	–6.15	–25.3	–6.17	–25.3
5	$\bar{\sigma}_\theta^e$	–12.923	–0.51	–1.54	–0.44	–1.47	$\bar{\sigma}_x^e$	–0.73423	–1.63	–5.94	–1.49	–5.81
10	$(-0.5h)$	–12.821	–0.31	–0.91	–0.29	–0.89	$(-0.5h)$	–0.71242	–0.86	–3.34	–0.83	–3.31
20		–12.762	–0.16	–0.48	–0.16	–0.48		–0.70050	–0.44	–1.77	–0.43	–1.76
40		–12.732	–0.09	–0.25	–0.09	–0.25		–0.69431	–0.22	–0.91	–0.22	–0.91
5	$\bar{\tau}_{\theta x}$	–0.090954	–2.90	–6.43	–1.59	–5.21	$\bar{\sigma}_\theta^p$	–1.0225	–14.0	–59.4	–14.2	–60.3
10	$(0.4h^+)$	–0.10173	–1.09	–2.89	–0.69	–2.55	$(0.4h^+)$	–0.79055	–14.4	–48.7	–14.6	–49.1
20		–0.10588	–0.45	–1.39	–0.35	–1.29		–0.63965	–13.1	–35.8	–13.2	–35.9
40		–0.10755	–0.20	–0.68	–0.18	–0.66		–0.55613	–11.7	–25.1	–11.7	–25.2
5	$\bar{\tau}_{\theta z}$	–0.15346	2.99	7.68	3.29	8.03	$\bar{\tau}_{\theta x}$	0.46301	4.45	15.4	4.07	15.0
10	$(-0.185h)$	–0.16911	1.40	4.00	1.47	4.08	$(-0.5h)$	0.49989	2.03	7.72	1.95	7.63
20		–0.17489	0.66	2.02	0.68	2.04		0.51953	0.97	3.85	0.95	3.83
40		–0.17717	0.32	1.01	0.33	1.02		0.52962	0.47	1.92	0.47	1.92
5	$\bar{D}_z$	0.096015	–22.3	–75.4	–23.5	–76.9	$\bar{\tau}_{xz}$	–0.15942	1.07	2.55	0.92	2.42
10	$(0.5h)$	0.070628	–21.0	–64.7	–21.5	–65.3	$(-0.275h)$	–0.16049	0.43	1.34	0.39	1.31
20		0.052848	–19.2	–50.7	–19.4	–50.9		–0.16052	0.19	0.69	0.18	0.68
40		0.042949	–17.7	–37.6	–17.7	–37.7		–0.16042	0.09	0.35	0.09	0.35
5							$\bar{D}_z$	0.17730	–11.2	–38.0	–11.4	–38.5
10							$(0.5h)$	0.15998	–10.2	–27.6	–10.3	–27.7
20								0.14759	–9.0	–19.1	–9.1	–19.2
40								0.14048	–8.2	–13.7	–8.2	–13.7

Table 6. Exact 3D results and percent errors of 2D theories for hybrid panels (a) and (b) under load case 3.

	Panel (c)					Panel (c)					
S	Entity	Exact	IZIGT	ZIGT	ITOT	TOT	Entity	Exact	IZIGT	ZIGT	ITOT	TOT
5	$\bar{u}_\theta$	–2.8779	–1.52	–24.7	–4.04	–26.9	$\bar{\tau}_{\theta x}$	1.7026	0.41	2.32	0.79	2.60
10	(–0.5h)	–2.2940	–0.82	–15.2	–1.61	–15.9	(–0.4h^+)	1.7444	0.19	1.06	0.29	1.13
20		–2.0141	–0.43	–8.50	–0.66	–8.68		1.7616	0.09	0.50	0.12	0.52
40		–1.8781	–0.23	–4.51	–0.29	–4.56		1.7692	0.04	0.24	0.05	0.25
5	$\bar{w}$	–3.7519	–1.98	–27.7	–4.78	–30.2	$\tau_{\theta z}$	0.26651	0.65	2.29	1.27	2.79
10	(–0.5h)	–3.1537	–0.97	–16.4	–1.81	–17.1	(0.4h)	0.26441	0.17	0.86	0.31	0.97
20		–2.8760	–0.48	–8.87	–0.71	–9.07		– 0.26246	0.05	0.37	0.09	0.39
40		–2.7442	–0.24	–4.62	–0.30	–4.67		– 0.26128	0.03	0.17	0.03	0.18
5	$\bar{\sigma}_\theta^e$	23.442	1.32	4.07	1.80	4.42	D_z	0.60796	–4.61	–8.00	–4.93	–8.37
10	(–0.4h^+)	24.247	0.63	1.87	0.75	1.96	(0.5h)	– 0.64232	–5.05	–6.99	–5.14	–7.09
20		24.591	0.31	0.90	0.34	0.92		– 0.65673	–5.25	–6.29	–5.28	–6.31
40		24.747	0.15	0.44	0.16	0.44		– 0.66318	–5.35	–5.89	–5.36	–5.89
5	$\bar{\sigma}_x^p$	–3.5722	0.39	1.95	0.75	2.21	$\bar{\phi}$	–58.181	1.39	0.29	1.49	0.35
10	(–0.5h)	–3.6373	–0.03	0.66	0.05	0.72	(–0.5h)	–58.563	0.65	0.13	0.67	0.14
20		–3.6638	–0.20	0.13	–0.18	0.14		–58.711	0.31	0.06	0.32	0.06
40		–3.6757	–0.27	–0.11	–0.26	–0.11		–58.775	0.15	0.03	0.15	0.03

Table 7. Exact 3D results and percent errors of 2D theories for hybrid sandwich panel (c) under load case 3.

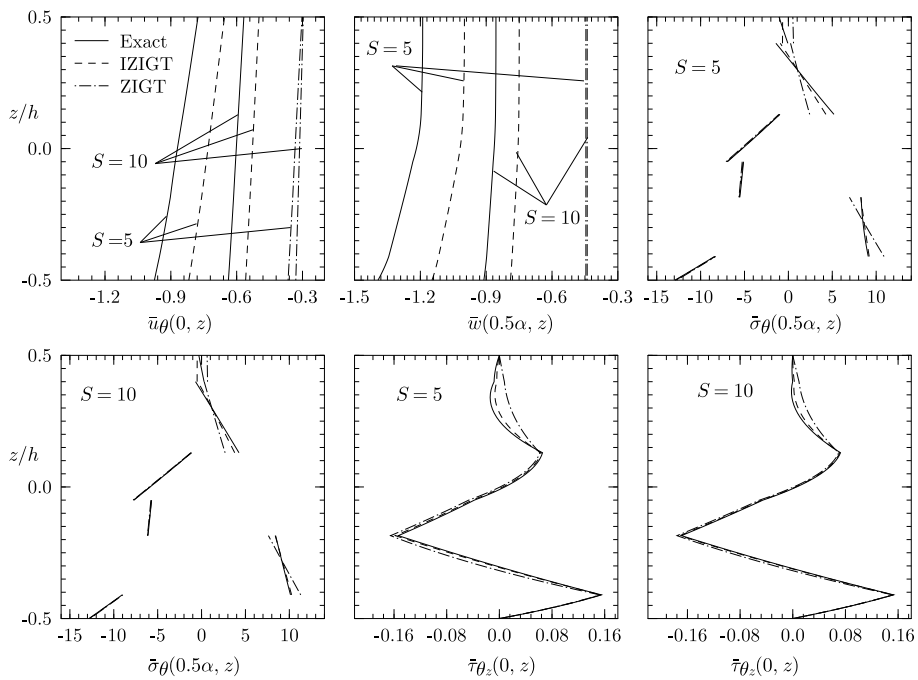

Figure 9. Through-the-thickness distributions of $\bar{u}_\theta$, $\bar{w}$, $\bar{\sigma}_\theta$, and $\bar{\tau}_{\theta z}$ for hybrid test panel (a) under load case 3.

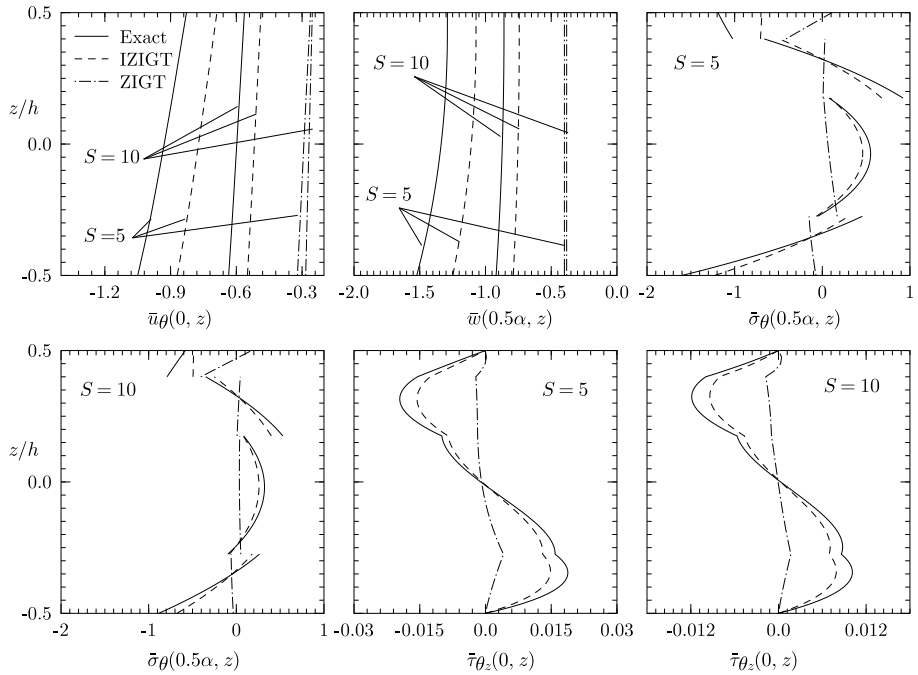

Figure 10. Through-the-thickness distributions of $\bar{u}_\theta$, $\bar{w}$, $\bar{\sigma}_\theta$, and $\bar{\tau}_{\theta z}$ for hybrid composite panel (b) under load case 3.

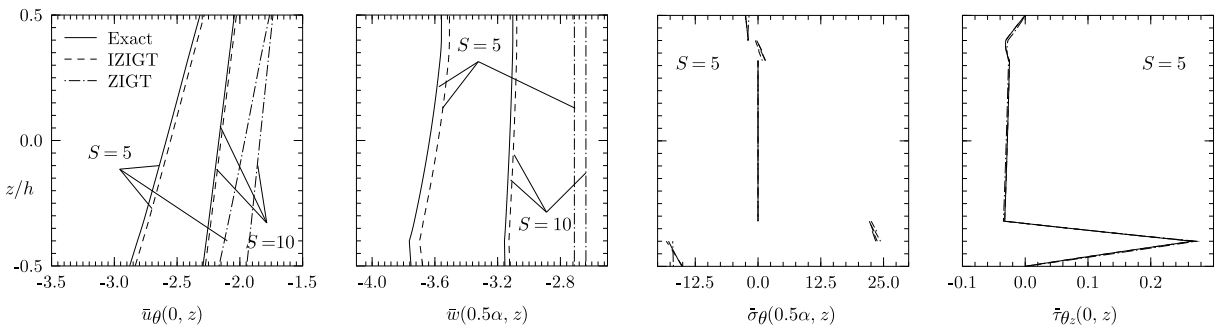

Figure 11. Through-the-thickness distributions of $\bar{u}_\theta$, $\bar{w}$, $\bar{\sigma}_\theta$, and $\bar{\tau}_{\theta z}$ for hybrid sandwich panel (c) under load case 3.

panels. These distributions show significant improvement for the IZIGT. The percent error in $\bar{w}$ and $\bar{\sigma}_\theta^e$ in the substrate is plotted in Figure 13 against the fibre axis angle ψ of the face layers of the sandwich panel (c) with span angle $\alpha = 2\pi/3$ and $S = 10$. The error in $\bar{w}$ for the ITOT and ZIGT (for the thermal load case) increases with the decrease in the ply angle ψ for all load cases, but the same does not hold well for $\bar{\sigma}_\theta^e$. For the IZIGT, the same trend is valid for $\bar{w}$ only for load case 1.

The effect of span angle α on the response is shown by plotting the % error in $\bar{w}$ and $\bar{\sigma}_\theta^e$ against the span angle in Figure 14 for the hybrid sandwich panel with $S = 10$ and $\psi = 30°$ under load cases 1–3. It is observed that the error in the ITOT and ZIGT (for the thermal load case) increases with the decrease in the span angle for all load cases. The same is not always true for the IZIGT for which the error is small.

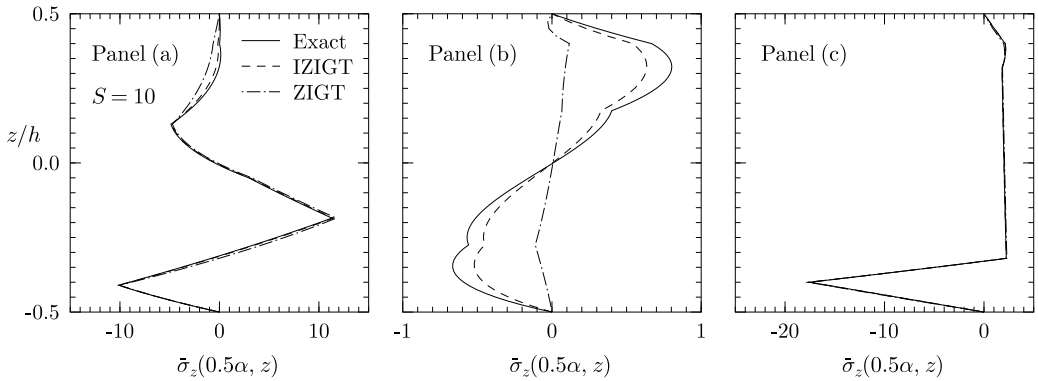

Figure 12. Through-the-thickness distributions of $\bar{\sigma}_z$ for panels (a), (b), and (c) under load case 3.

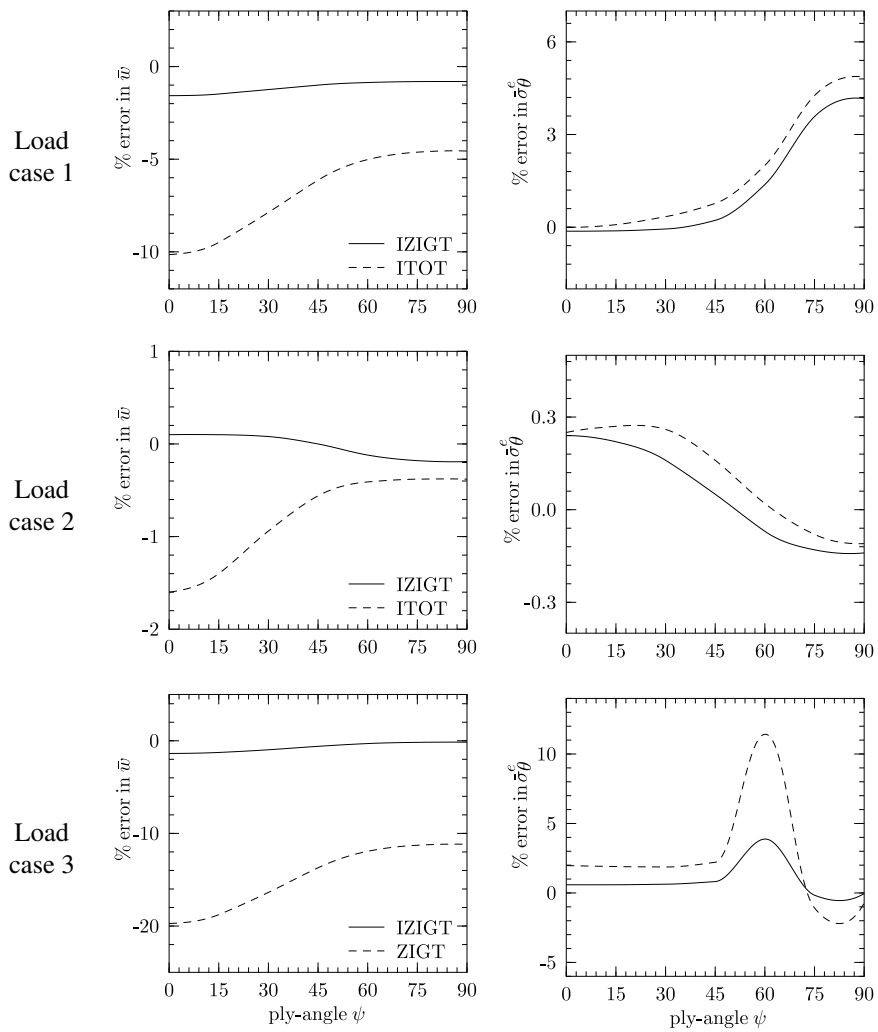

Figure 13. Effect of ply angle on percent error of $\bar{w}$ and $\bar{\sigma}^e_\theta$ for hybrid panel (c).

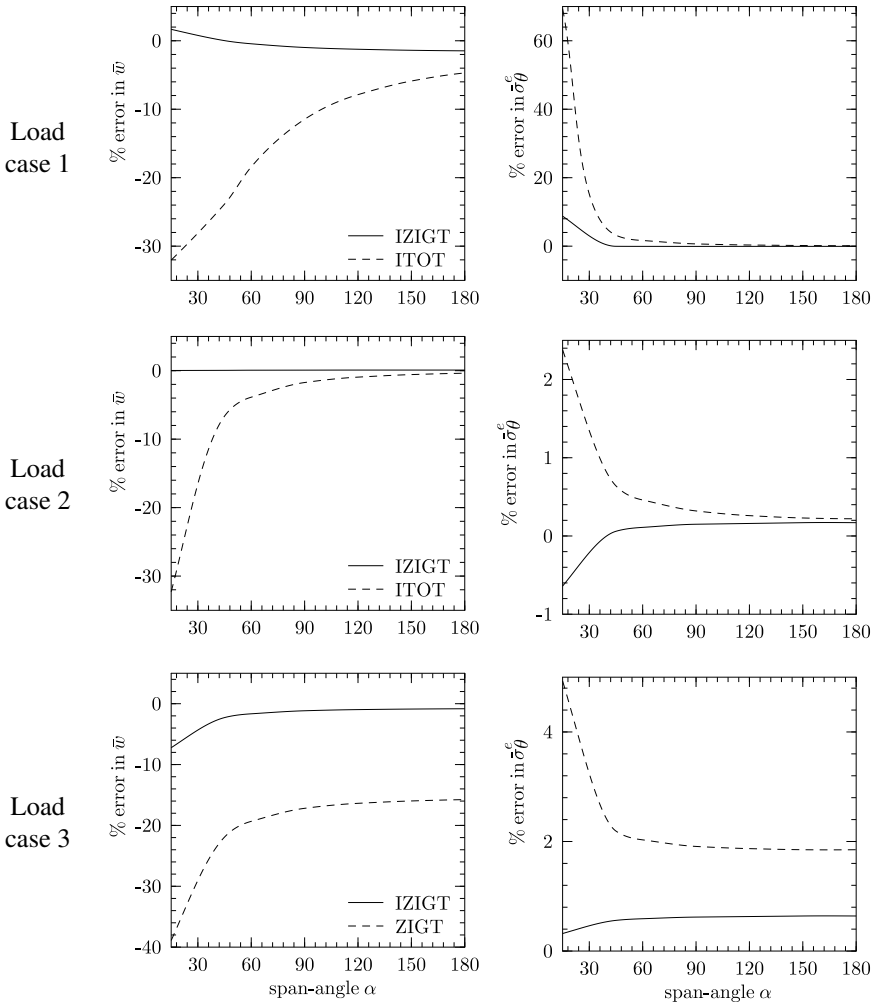

Figure 14. Effect of span-angle on percent error of $\bar{w}$ and $\bar{\sigma}_\theta^e$ for hybrid panel (c).

7. Conclusions

An improved third-order zigzag theory and an improved third-order theory have been presented for the electrothermomechanical response of hybrid angle-ply circular cylindrical shells. The accuracy of the theories has been assessed in direct comparison with the 3D exact piezothermoelasticity solution for simply supported infinite-length angle-ply cylindrical panels under pressure, electric potential, and thermal loads. The assessment is made for hybrid shell panels with highly inhomogeneous test, composite, and sandwich substrates. Based on the assessment of maximum values of entities and their distributions across the thickness, it is concluded that the IZIGT with the same number of unknowns as the ITOT yields accurate results and is a significant improvement over the ITOT for all laminate configurations for mechanical and potential loads. This improvement is due to the inclusion of layerwise terms in the approximation of inplane displacements in the IZIGT. However, the IZIGT and ITOT do not show any

significant differences for the thermal loading case. Both the theories, however, show significant improvements over their counterparts with uniform w across the thickness for thermal loads. The inclusion of the transverse normal strain in the approximation of w in the 2D theories improves not only the predicted deflection but all other response entities. In general, the error in the ITOT increases with the decrease in ply angle and span angle. The same does not hold well for the IZIGT for which the error itself is small.

References

[Auld 1973] B. A. Auld, *Acoustic fields and waves in solids*, vol. I, John Wiley, New York, 1973.

[Berg et al. 2004] M. Berg, P. Hagedorn, and S. Gutschmidt, "On the dynamics of piezoelectric cylindrical shells", *J. Sound Vib.* **274**:1–2 (2004), 91–109.

[Carrera 2002] E. Carrera, "Temperature profile influence on layered plates response considering classical and advanced theories", *AIAA J.* **40**:9 (2002), 1885–1896.

[Carrera and Brischetto 2007] E. Carrera and S. Brischetto, "Reissner mixed theorem applied to static analysis of piezoelectric shells", *J. Intell. Mater. Syst. Struct.* **18**:10 (2007), 1083–1107.

[D'Ottavio et al. 2006] M. D'Ottavio, D. Ballhause, B. Kroplin, and E. Carrera, "Closed-form solutions for the free-vibration problem of multilayered piezoelectric shells", *Comput. Struct.* **84**:22–23 (2006), 1506–1518.

[Dumir et al. 1997] P. C. Dumir, G. P. Dube, and S. Kumar, "Piezothermoelastic solution for angle-ply laminated cylindrical panel", *J. Intell. Mater. Syst. Struct.* **8**:5 (1997), 452–464.

[Jia and Rogers 1990] J. Jia and C. A. Rogers, "Formulation of a laminated shell theory incorporating embedded distributed actuators", *J. Mech. Des.* (*ASME*) **112**:4 (1990), 596–604.

[Kapuria and Achary 2006] S. Kapuria and G. G. S. Achary, "Electromechanically coupled zigzag third-order theory for thermally loaded hybrid piezoelectric plates", *AIAA J.* **44**:1 (2006), 160–170.

[Kapuria et al. 1997] S. Kapuria, P. C. Dumir, and S. Sengupta, "Nonaxisymmetric exact piezothermoelastic solution for laminated cylindrical shell", *AIAA J.* **35**:11 (1997), 1792–1795.

[Kapuria et al. 1998a] S. Kapuria, P. C. Dumir, and S. Sengupta, "Assessment of shell theories for hybrid piezoelectric cylindrical shell under thermoelectric load", *J. Therm. Stresses* **21**:5 (1998), 519–544.

[Kapuria et al. 1998b] S. Kapuria, S. Sengupta, and P. C. Dumir, "Assessment of shell theories for hybrid piezoelectric cylindrical shell under electromechanical load", *Int. J. Mech. Sci.* **40**:5 (1998), 461–477.

[Kim et al. 2002] H. S. Kim, X. Zhou, and A. Chattopadhyay, "Interlaminar stress analysis of shell structures with piezoelectric patch including thermal loading", *AIAA J.* **40**:12 (2002), 2517–2525.

[Kumari et al. 2008] P. Kumari, J. K. Nath, S. Kapuria, and P. C. Dumir, "An improved third order theory and assessment of efficient zigzag theory for angle-ply flat hybrid panels", *Compos. Struct.* **83**:2 (2008), 226–236.

[Lee and Saravanos 2000] H. J. Lee and D. A. Saravanos, "A mixed multi-field finite element formulation for thermopiezoelectric composite shells", *Int. J. Solids Struct.* **37**:36 (2000), 4949–4967.

[Oh and Cho 2007] J. Oh and M. Cho, "Higher order zig-zag theory for smart composite shells under mechanical-thermo-electric loading", *Int. J. Solids Struct.* **44**:1 (2007), 100–127.

[Ossadzow-David and Touratier 2004] C. Ossadzow-David and M. Touratier, "A multilayered piezoelectric shell theory", *Compos. Sci. Technol.* **64**:13–14 (2004), 2121–2137.

[Pinto Correia et al. 2002] I. F. Pinto Correia, C. M. Mota Soares, C. A. Mota Soares, and J. Herskovits, "Active control of axisymmetric shells with piezoelectric layers: a mixed laminated theory with a high order displacement field", *Comput. Struct.* **80**:27–30 (2002), 2265–2275.

[Raja et al. 2004] S. Raja, P. K. Sinha, G. Prathap, and D. Dwarakanathan, "Thermally induced vibration control of composite plates and shells with piezoelectric active damping", *Smart Mater. Struct.* **13**:4 (2004), 939–950.

[Saravanos 1997] D. A. Saravanos, "Mixed laminate theory and finite element for smart piezoelectric composite shell structures", *AIAA J.* **35**:8 (1997), 1327–1333.

[Saravanos and Christoforou 2002] D. A. Saravanos and A. P. Christoforou, "Low-energy impact of adaptive cylindrical piezoelectric-composite shells", *Int. J. Solids Struct.* **39**:8 (2002), 2257–2279.

[Saravanos and Heyliger 1999] D. A. Saravanos and P. R. Heyliger, "Mechanics and computational models for laminated piezoelectric beams, plates and shells", *Appl. Mech. Rev.* (*ASME*) **52**:10 (1999), 305–320.

[Sung et al. 1996] C. K. Sung, T. F. Chen, and S. G. Chen, "Piezoelectric modal sensor/actuator design for monitoring/generating flexural and torsional vibrations of cylindrical shells", *J. Vib. Acoust.* (*ASME*) **118**:1 (1996), 48–55.

[Tiersten 1969] H. F. Tiersten, *Linear piezoelectric plate vibrations: elements of the linear theory of piezoelectricity and the vibrations of piezoelectric plates*, Plennum Press, New York, 1969.

[Tzou and Bao 1995] H. S. Tzou and Y. Bao, "A theory on anisotropic piezothermoelastic shell laminates with sensor/actuator applications", *J. Sound Vib.* **184**:3 (1995), 453–473.

[Xu and Noor 1996] K. Xu and A. K. Noor, "Three-dimensional analytical solutions for coupled thermoelectroelastic response of multilayered cylindrical shells", *AIAA J.* **34**:4 (1996), 802–812.

[Zhang et al. 2008] Y. H. Zhang, S. L. Xie, and X. N. Zhang, "Vibration control of a simply supported cylindrical shell using a laminated piezoelectric actuator", *Acta Mech.* **196**:1–2 (2008), 87–101.

Received 24 Jan 2009. Revised 27 Mar 2009. Accepted 31 Mar 2009.

JAYANTA KUMAR NATH: jkniter@gmail.com
Department of Applied Mechanics, Indian Institute of Technology Delhi, New Delhi 110016, India

SANTOSH KAPURIA: kapuria@am.iitd.ac.in
Department of Applied Mechanics, Indian Institute of Technology Delhi, New Delhi 110016, India
http://web.iitd.ac.in/~am/